Aalto University
School of Science

Juha Peltonen

Cardiovascular magnetic resonance imaging: Error sources in phase contrast flow measurements

Licentiate thesis submitted in partial fulfillment of the requirements for the degree of Licentiate of Science in Technology

Espoo, 15.7.2013

Supervisor: Professor Risto Ilmoniemi

Instructor: Docent Outi Sipilä

Aalto University
School of Science

Aalto University, P.O. BOX 11000, 00076 AALTO
www.aalto.fi

Abstract of licentiate thesis

Author Juha Peltonen

Title of thesis Cardiovascular magnetic resonance imaging: Error sources in phase contrast flow measurements

Department Department of Biomedical Engineering and Computational Science

Field of research Biomedical Engineering

Supervising professor Prof. Risto Ilmoniemi **Code of professorship** F036Z

Thesis advisor(s) Doc. Outi Sipilä

Thesis examiner(s) PhD. Eveliina Lammentausta

Number of pages 77 **Language** English

Date of submission for examination 21.3.2013

Abstract

Phase contrast velocity encoded flow measurement was first introduced 30 years ago and have been subject to constant evolution since. The method has been validated repeatedly to be suitable for numerous clinical applications. It is capable to visualize and quantify dynamic phenomena such as blood flow in any part of the human body without being invasive or using ionizing radiation. Recent publications even suggest that velocity encoded imaging should be used as a gold standard in the flow measurements of great arteries. Despite of numerous possibilities, the method remains underused.

However, phase contrast flow imaging carries some challenges that are limiting clinical applicability. First of all, magnetic resonance imaging is expensive and time consuming imaging modality. Currently velocity encoded flow imaging can be seen as a secondary modality which is used if necessary after alternative methods such as ultrasound. Also, phase contrast flow imaging includes numerous physical and physiological error sources affecting the accuracy of flow measurements. The understanding of these error sources is important to be able to estimate the accuracy of obtained results. An overview on these error sources is presented in this work. Essential theoretical basis to understand the physics underlying the error mechanisms are presented and means to minimize the error are addressed.

The dimensions of human arteries are varying considerably along the flow track beyond the ventricles. Changing geometrical dimension and individual characteristics of cardiac valves are giving a raise to several spatially alternating flow phenomena such as acceleration artefact and voxel dephasing. In this work a research is presented where optimal measurement plane to quantify stroke volume is studied. The importance of optimal measurement plane is studied in both healthy controls and patients with accelerated flow velocities. In the work it was found that optimal location to measure arterial flow is approximately 2 cm distal from the aortic or pulmonal valve in case of accelerated flow. In controls no such relation was found between the measurement plane and the stroke volume. We are also considering the amount of hardware velocity offset in our measurement system and discussing how it affects to the results.

Keywords MRI, phase contrast flow imaging

Tekijä Juha Peltonen

Työn nimi Sydämen magneettikuvaus: Virhelähteet virtausten vaihekontrastimittauksissa

Laitos Lääketieteellisen tekniikan ja laskennallisen tieteen laitos

Tutkimusala Lääketieteellinen tekniikka

Vastuuprofessori Prof. Risto Ilmoniemi **Professuurikoodi** F036Z

Työn ohjaajat Dos. Outi Sipilä

Työn tarkastajat FT Eveliina Lammentausta

Jätetty tarkastettavaksi 21.3.2013 **Sivumäärä** 77 **Kieli** Englanti

Tiivistelmä

Nopeusherkkään vaihekontrastiin perustuva magneettikuvausmenetelmä on tehokas tapa suurten valtimoiden virtausten tutkimiseen. Menetelmällä on mahdollista määrittää virtauksen nopeus missä tahansa paikassa ja suunnassa ihmiskehossa ilman ionisoivaa säteilyä tai kajoamista kehon sisälle. Nykytutkimuksen valossa nopeusherkkiä vaihekontrastimittauksia pidetään erilaisten sydänsairauksien arviointiperusteena. Menetelmän kiistattomista eduista huolimatta sitä käytetään tällä hetkellä huomattavan vähän.

Nopeusherkän vaihekontrastikuvantamisen kliinistä käyttöä rajoittavat haasteet sovellettavuudessa jokapäiväiseen sairaalatyöhön. Magneettikuvaus itsessään on tällä hetkellä suhteellisen kallis tutkimusmodaliteetti ja sitä on pidettävä sydänsairauksien osalta toisen linjan kuvantamisemenetelmänä ultraäänitutkimuksen jälkeen. Itse nopeusherkkään vaihekontrastiin perustuva kuvantaminen on altis useille fysikaaliseen perustaan ja ihmisen fysiologiaan liittyville virhelähteille. Esimerkiksi kiihtyneessä valtimoverenkierrossa syntyvät turbulenssit ja sydämen rytmihäiriöt saattavat aiheuttaa merkittävää virhettä mitattuihin tuloksiin. Tässä työssä on tehty kirjallisuustutkimus, jossa eritellään nopeusherkällä vaihekontrastikuvantamisella saatuihin tuloksiin vaikuttavat virhemekanismit. Lisäksi käydään läpi mekanismien taustojen ymmärtämiseen vaadittava teoria ja esitellään keinoja syntyvän virheen minimoimiseksi.

Suurissa valtimoissa kulkevan veren virtauksen luonne on vahvasti paikkariippuvaista. Näin ollen mitattaessa sydämen tunnuslukuja nopeusherkkään vaihekontrastiin perustuvalla menetelmällä on mittaukseen käytettävän kuvatason paikalla merkittävä vaikutus tuloksiin. Kuvatason paikan vaikutusta mitattuun sydämen vasemman ja oikean kammion iskutilavuuteen on selvitetty kokeellisessa tutkimuksessa. Saatujen tulosten mukaan optimaalinen kuvatason paikka sijaitsee noin 2 cm etäisyydellä valtimoläpästä distaalisesti potilailla joilla on kiihtynyt valtimoveren virtaus. Terveillä koehenkilöillä ei kuvatason paikalla havaittu olevan merkittävää vaikutusta mitattuun kammion iskutilavuuteen. Tutkimuksessa käsitellään lisäksi kokeellisessa osassa käytetyn laitteiston aiheuttamaa virhettä tuloksiin.

Avainsanat magneettikuvaus, virtausten vaihekontrastikuvantaminen

Acknowledgements

I would like to thank my instructor Outi Sipilä for valuable counseling over the course of writing this thesis. Without her precise observations I would have not gotten so many important insights during the process. I do also owe a thanks to all my superiors in HUS for the possibility to work in interesting hospital environment.

Radiologists Miia Holmström, Sari Kivistö and Kirsi Lauerma are also deserving a big thank you for initiating me to the secrets of cardiovascular imaging. Most of all I have to give credit for my fellow medical physicist Touko Kaasalainen for tutoring me on the subject from day one.

Finally, I would like to thank all my colleagues who I have been privileged to work with during the past four years. You make me push ahead on those days when you keep falling off the shoulders of giants no matter how hard you try.

Contents

Abbreviations

ECG	Electrocardiography
FOV	Field of view
G_F	Frequency encoding gradient
G_P	Phase encoding gradient
G_S	Slice selection gradient
MRI	Magnetic resonance imaging
RF	Radiofrequency
ROI	Region of interest
SAR	Specific absorption rate
SNR	Signal to noise ratio
T_1	Longitudinal relaxation time constant
T_2	Lateral relaxation time constant
T_E	Echo time
T_R	Repetition time
TOF	Tetralogy of Fallot
UTE	Ultra short echo time
V_{ENC}	Maximum unambiguously encoded velocity
VCG	Vectorcardiography

1. Introduction

1.1. Introduction to cardiovascular flow measurements

Phase contrast velocity encoded flow measurement was first introduced by Moran et al [1] 30 years ago and have been subject to constant evolution since. The method has been validated repeatedly in numerous clinical applications [2-5]. It is capable to visualize and quantify dynamic phenomena such as blood flow in any part of the human body without being invasive or using ionizing radiation [6, 7]. Recent publications even suggest that velocity encoded imaging should be used as a gold standard in the flow measurements of the great arteries [8]. Despite numerous possibilities, the method is still at the edge of a great breakthrough and remains underused [9].

However, the method carries some challenges that are limiting clinical applicability. First of all, magnetic resonance imaging (MRI) is an expensive and time consuming imaging modality. Currently, velocity encoded flow imaging can be seen as a secondary modality which is used if necessary after primary methods such as ultrasound [10, 11]. Also, phase contrast flow imaging includes numerous physical and physiological error sources affecting the accuracy of the flow measurements. Understanding of these error sources is important to be able to estimate the accuracy of obtained results. The physics lying under the method is presented in Chapter 2. In Chapter 3 each error source is reviewed and the means to minimize the error is addressed.

The blood flow track from the ventricles to the great arteries is complex. Variable geometrical dimensions and individual characteristics of cardiac valves are inflicting flow phenomena. With spatially changing nature of flow, it is likely that also the amount of error in the flow study is changing depending on measurement location. It is presumed that there is an location in arterial flow path where the amount of measurement error is minimized. The position of an optimal plane to measure the stroke volume is studied in Chapters 4-6. The effect of the measurement plane location is studied in both healthy controls and patients with flow velocities of 250-500 cm/s. The amount of hardware velocity offset in our measurement system is also estimated and discussed how it contributes to the results.

1.2. Current phase contrast velocity encoded imaging applications

Phase contrast velocity encoded imaging provides two dimensional (2D) velocity profiles at any point of cardiac cycle anywhere within human body. In clinical use, typical application is flow imaging in difficult locations where no other measurement modality is applicable. Also, when the exact geometrical dimensions of the flow are needed, the spatial accuracy of the MRI is superior in comparison with other methods. [5, 12-18]

Basically, in phase contrast velocity encoded imaging the brightness of a voxel corresponds to the amount of the flow velocity. An example image can be seen in Figure 1. The techniques that are applied today in clinical routine are commonly 2D, where velocity encoding may take place either along the direction of the selected image plane (in-plane) or in the orthogonal direction to the image plane (through-plane). The flow velocity can be mapped in several directions during single imaging sequence but usually only one direction is used to save scanning time. In-plane techniques are more suitable for displaying the velocities along the whole flow track, whereas through-plane techniques are utilized for quantifying flow through a vessel section of interest. If the whole pumping cycle of the heart is imaged with suitable time steps, the velocity profile through the whole R-R interval can be formed in the selected slice.

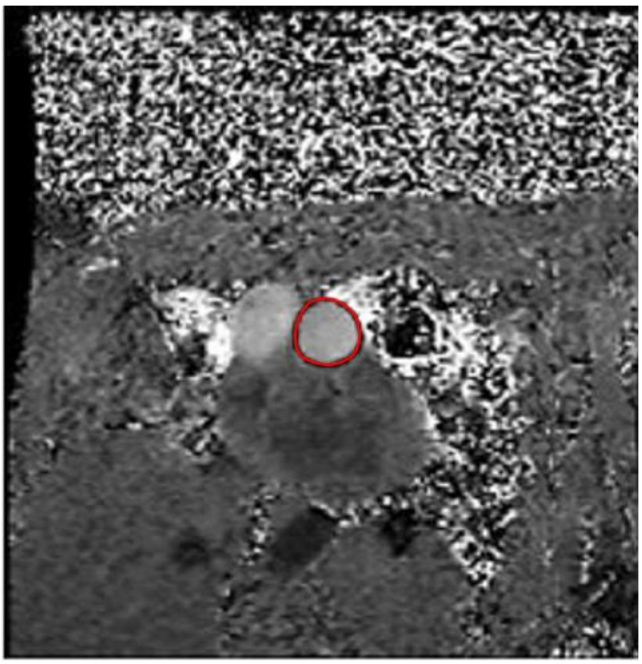

Figure 1. An example of through-plane phase contrast velocity encoded image. Aorta is circulated with a red circle.

Velocity maps are important tool in the assessment of stenosis where the speed of aortic or pulmonal flow is increased due to narrow ventricular outflow track. In these cases the speed of the flow and the size of the vessel lumen are important decision making factors. The known velocity profile and the dimensions of the stenosis can be utilized further to calculate the pressure gradient over the narrowing. [2, 19]

When the speed of the flow rises, the flow often becomes more complicated and turbulent. This is normally a problem in quantitative flow measurements. However, from a physiological point of view it is interesting to know if vortexes exist in flow. Dyverfeldt et al. have presented study on how to use specially tailored phase contrast imaging sequence to quantify the amount of complexity in flow [20].

Instantaneous flow volume of a vessel can be derived from through-plane images by multiplying the velocity of each pixel by the dimensions of the pixel and integrating the result over the vessel cross section. The flow volume through a vessel cross section can be plotted over time as a diagram (Figure 2). Integration of the area under the curve over the R-R interval delivers the total stroke volume. Stroke volume is an essential parameter in ventricular function assessment and a decrease in the value is seen as a

sign of cardiac dysfunction. The phase contrast velocity encoded imaging has been validated to be a very accurate and reproducible method to measure stroke volume. [8, 18, 21]

While it is important to know how much blood is pumped into the arterial system, it is at least equally important to know if there is blood leaking back to the heart during the diastolic phase of the heart. This valve regurgitation is an important functional sign of valve misfunction and can be effectively assessed with a flow volume measurement. The value that is used to quantify the state of regurgitation is the regurgitant fraction, which is calculated with equation

$$Regurgitant\ fraction = \frac{systolic\ forward\ flow\ volume}{regurgitant\ flow\ volume}. \quad (1)$$

The magnetic resonance phase contrast flow measurement is considered the gold standard for measuring regurgitation in aortic and pulmonary valves. [16, 22-26]

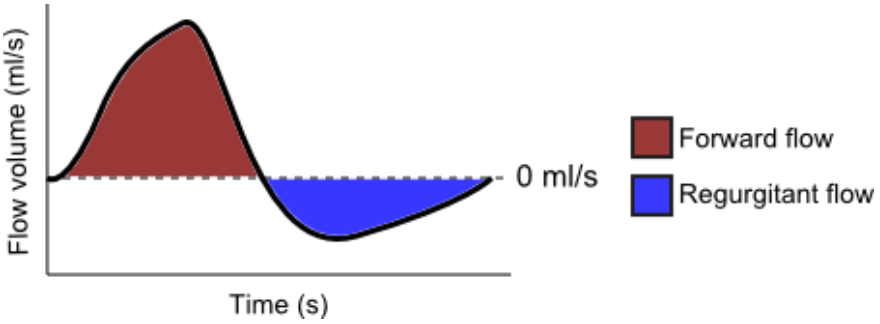

Figure 2. Illustration of the forward and regurgitant flow volumes within a R-R interval in the measurement plane.

The methods provided by the phase contrast flow imaging are especially beneficial for patients with congenital heart diseases, especially the tetralogy of Fallot (TOF). TOF usually involves three out of four typical morphological alterations that are pulmonar stenosis, overriding aorta, hole between the ventricles and right ventricular hypertrophy as presented in Figure 3. The first three are strongly affecting the flow in the heart and can be quantified with phase contrast flow imaging. Often TOF is repaired surgically within the first year of infant´s life. However, the progress of the disease has to be controlled over the whole adolescence, which would not be possible with an imaging modality utilizing ionizing radiation. Common complications that may develop

substantial in later life include residual stenosis of pulmonary valve and pulmonary valve regurgitation. These values are most reliably obtained with phase contrast velocity encoded imaging. [17, 27-32]

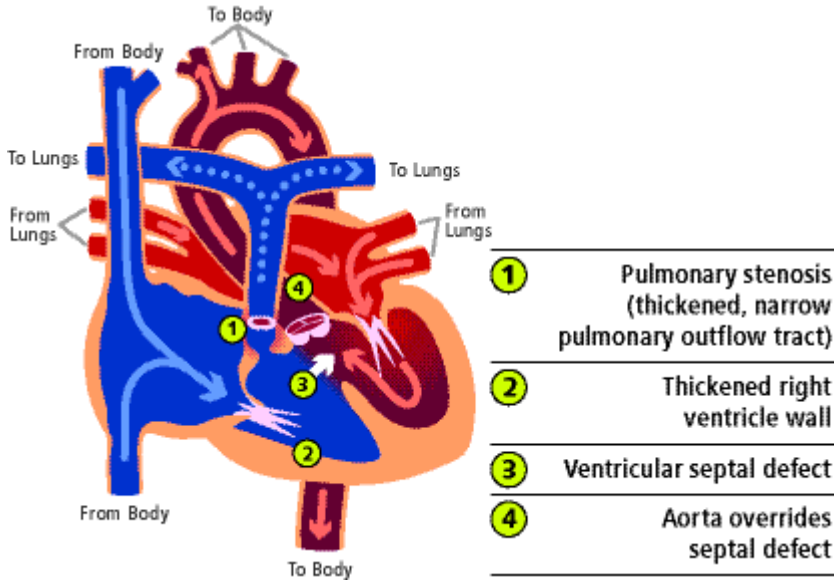

Figure 3. Anatomy of the tetralogy of Fallot. Adopted from [33].

Recent developments in MRI scanner technology and computational power have permitted the use of more complex imaging sequences enabling extensive studies in clinically applicable timeframe. In the field of cardiac phase contrast flow imaging the best example is the emerge of the four dimensional (4D) flow imaging. The four dimensions mean that the complete flow vector can be solved for each voxel in a volume for the whole R-R time period. 4D imaging is often accompanied with advanced post processing enabling e.g. particle tracing. An example of a 4D visualization of the blood flow in aorta can be seen in Figure 4. Multidimensional imaging is especially useful when flow patterns are studied as ensembles. For example, the vortexes and turbulentic progression inflicted by a faulty aortic valve can be tracked through the whole span of ascending aorta. [25, 34-39]

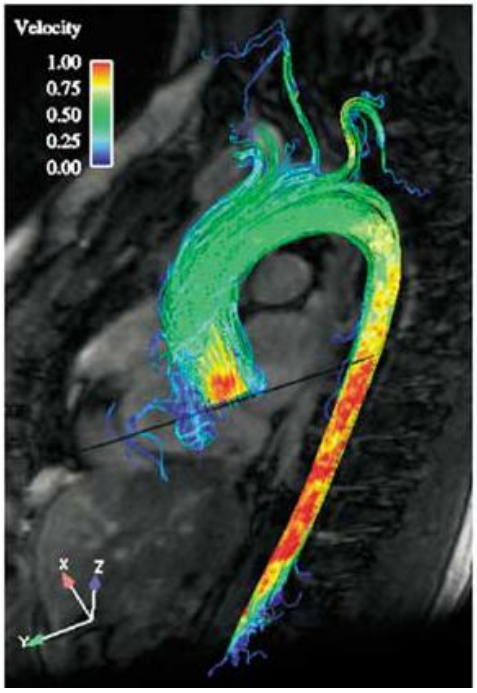

Figure 4. Illustration of 4D imaging capabilities in visualizing aortic flow. Adopted from [36].

1.3. Alternative methods

Fick´s method, introduced by Adolf Fick in 1870, is probably the oldest credible method of measuring the cardiac output or the blood volume pumped by the heart in the time interval of one minute. The method is based on an assumption that the amount of oxygen consumption of a body is equal to the product of blood flow and the oxygen content difference between the arterial and venous blood. Based on that principle an equation can be formed

$$Cardiac\ output = \frac{Oxygen\ uptake}{Arterio{-}venous\ oxygen\ content\ difference}. \quad (2)$$

Indicator dilution technique is a similar method to the Fick´s principle which is based on the injecting marked solution to the blood stream and measuring how the concentration of the solution is varying at certain point downstream. Typically, known amount of cold fluid is injected with a catheter to the blood stream near the entrance of right atrium. [23, 40]

Bioimpedance based methods of measuring cardiac output are relying on an assumption that electrical properties in human body are related to the amount of cardiac blood flow volume. These bioimpedances are measured by applying low-voltage current with high-frequency to thorax through contact electrodes. With known current, voltage and frequency, impedance between electrodes can be calculated. This impedance can be substituted in a formula which then returns a value for cardiac output. However, using limited number of measured values to model the cardiac output is restricting the accuracy of the method. [40, 41]

Using ultrasound to measure the cardiac output and ejection fraction is based on the ability to measure both anatomical dimensions and the speed of the flow. The measurement of flow speed is based on the Doppler effect which states that the frequency of propagating waves is changed if they are reflected from a moving surface. When also the cross sectional area of the aortic orifice can be determined from the ultrasound images, the amount of blood flow relative to the time can be calculated by multiplying the speed of the flow by the orifice area. The greatest advantage of ultrasound is affordability and easy applicability without a requirement for special study

room. However, often the anatomical structures are limiting the views available for ultrasound and thus making the direct measurement of flow parameters impossible. [40]

In addition to phase contrast velocity encoded flow imaging there is another method of quantifying cardiac output with the MRI. This method, called magnetic resonance volumetry, is entirely based on mapping of the inner walls of the ventricles from anatomical images (Figure 5). If the largest volume of the ventricle during the systolic phase and the smallest volume during the systolic phase of the heart cycle is known, the stroke volume of the heart can be calculated by subtracting the two.

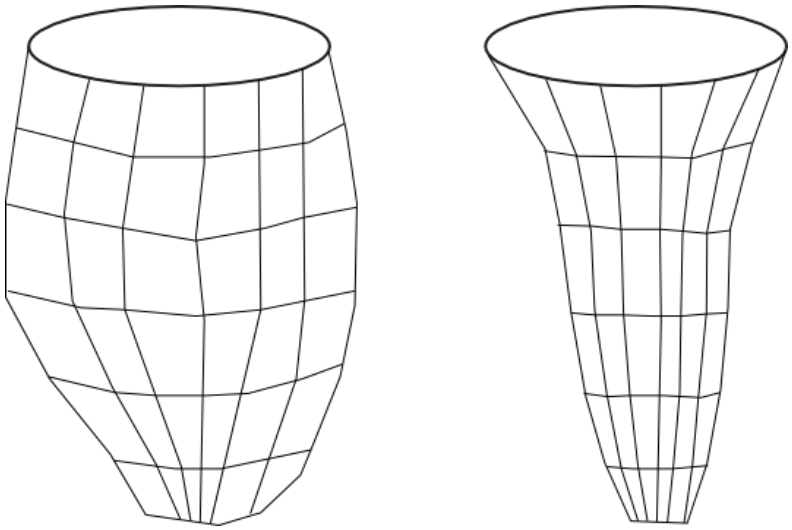

Figure 5. Left ventricle 3D model in diastole (left) and systole (right).

Ideally, volumetry should work perfectly as a method of quantifying cardiac output and ejection fraction. In practice however, as the method is based on pure subtraction, it counts on a perfect operation of the heart valves. If there is any regurgitation present in the pumping process, it is not taken into account in the stroke volume. In that respect it is justified to say that magnetic resonance volumetry provides the stroke volume value that is representing the best possible situation. [21]

Both single photon emission tomography (SPECT) and positron emission tomography (PET) modalities are able to quantify volumes of the left ventricle [42, 43]. Both imaging modalities are based on the injection of radioactive isotope solution which then accumulates to the target tissue. This concentration can be imaged with respective

detectors and an image computed from the data. The accumulation distribution depends on the used pharmaceutical agent which is bonded with the radioactive isotope. The calculations of all volumes are based on a model of the ventricle that is fitted to the radioisotope image. If the signal to noise ratio (SNR) of the image is low or defected parts of the heart do not collect the imaging agent, the ventricle model is becoming distorted and an error is produced to the measured values. Also, it has to remembered that radioisotopes are emitting ionizing radiation and thus are producing some radiation dose to the patient.

2. Theory

2.1. Magnetic resonance imaging

2.1.1. Signal origins

MRI is based on the manipulating nucleus magnetic moments i.e. spins. Non-zero spin, which is a requirement for nuclear magnetic resonance activity, exists only in nuclei with either an odd mass or odd atomic number or both. Majority of the MRI is based on the hydrogen nucleus which is satisfying this condition and also the most common nucleus in human body. When hydrogen nucleus is placed in magnetic field its spins will align with the field. The alignment of the spins generates a net magnetization which can be described by equation

$$M_0 = \frac{\rho_0 \gamma^2 h^2}{4 k_B T} B_0 \ , \tag{3}$$

where B_0 is the strength of external magnetic field, T is the ambient temperature, ρ_0 is the density of spins in unit volume, γ is the gyromagnetic ratio, the h is Planck´s constant and k_B is Boltzmann´s constant. The thermal equilibrium net magnetization is aligned paraller to the main field if it is left undistracted.

In an external magnetic field, spins rotate around the main magnetic field axis with the Larmor frequency

$$f_0 = \frac{\gamma}{2\pi} B_0 \ , \tag{4}$$

which states that the frequency is proportional to the main magnetic field strength B_0 and gyromagnetic ratio γ specific for each nucleus.

Only the time varying part of the magnetization perpendicular to main magnetic field is capable of inducing a signal in the receiving coil. This component of the magnetization is referred as the transversal component in oppose to the longitudinal component, which is parallel to the main magnetic field. In order to generate a MRI signal, the magnetization must be tipped at away from thermal equilibrium so that the magnetization lies at least partially in the transverse plane. To achieve this, the spins are

exposed to a radiofrequency (RF) magnetic field with frequency equal to the Larmor frequency. The flip angle of the net magnetization vector is controlled by modulating the strength and duration of a RF pulse. When the RF pulse is switched on, the net magnetization begins to move away from its alignment with the main magnetic field and rotate around it. [44-47]

2.1.2. Relaxation

Immediately after the RF pulse, the net magnetization starts to return to thermal equilibrium. This process is known as relaxation. Relaxation can be divided in to two distinct processes: The first is the return of net magnetization into alignment with the main magnetic field which is generally referred to longitudinal or T_1 relaxation according to the time constant describing the process. The longitudinal relaxation of the net magnetization vector M_0 parallel to the external magnetic field can be described by the equation

$$M_Z = M_0(1 - e^{-\frac{t}{T_1}}) \ , \tag{5}$$

where *t* is the time from signal excitation. A graphical illustration of the T_1 decay is presented in the Figure 6.

The second, usually faster, relaxation process is due to the loss of phase coherence between spins. Correspondingly, this relaxation process is generally referred to transversal or T_2 relaxation. The transversal magnetization vector M_{xy} in x-y plane can be described with time constant T_2 as

$$M_{XY} = M_0 e^{-\frac{t}{T_2}} \ . \tag{6}$$

In reality the decay is even more rapid than predicted by the time constant T_2 due to the actual relaxation is taking place according to time constants T_2* as illustrated in Figure 6. The T_2*decay is resulting from the variations in the magnetic field. Even with absolutely uniform magnetic field, the introduction of tissue into the field would produce subtle local changes in the magnetic field strength.

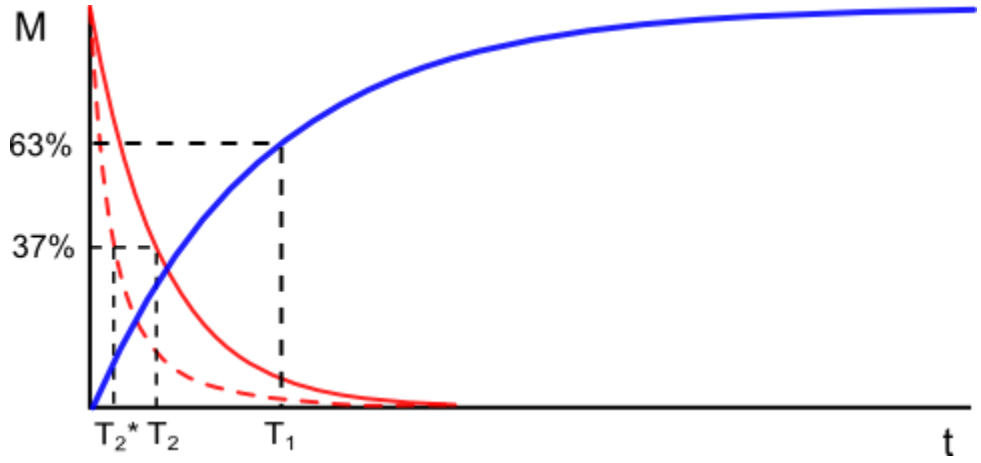

Figure 6. Illustration of T_1, T_2 and T_2 relaxation.*

T_1 and T_2 values are strongly dependent on the tissue properties. Additionally, T_1 values are varying corresponding to the strength of the main magnetic field. In T_2 the dependency on the magnetic field strength is weak, but small changes can be observed. [44-47]

2.1.3. Signal localization

The received signal can be characterized by its frequency and phase as well as by its intensity. To form magnetic resonance images, it is necessary to determine the location of the signal through some form of spatial encoding scheme. This is done by using a non-uniform magnetic field which causes local net magnetization to be encoded in terms of its precession frequency and phase. The non-uniform fields are generated through the application of time-dependent magnetic field gradients.

A typical 2D pulse sequence is often started by applying the slice selection gradient G_S. The magnetic field is made slightly non-uniform perpendicular to the desired image plane by supplying power to the respective gradient coils. Desired image plane can be selected by applying a narrow band RF pulse. Only the protons in specific plane with corresponding frequency will absorb the energy from the RF field and induce the flipping of the net magnetization.

The phase encoding gradient G_P is applied along the Y axis. The purpose of this gradient is to speed up the precession of the protons proportional to their location

respective to the Y axis. When the gradient is switched off, each proton returns to precess at the original frequency, but with location dependent phase shift.

The readout, or frequency encoding gradient G_F, is applied along the X axis of the selected slice. This gradient will cause the protons to precess at a slightly higher frequency where the field is stronger and slightly lower frequency where the field is weaker respectively. The signal is now accommodating a band of frequencies from the slice previously excited, where each individual frequency is corresponding to a line in the slice.

After applying the gradients, the time domain magnetic resonance signal is sampled in the frequency space or so called k-space in the context of MRI. The location in k-space, where the signal is recorded to, is depending on the frequency and phase shifts generated by the gradients (Figure 7). Each sample in the k-space contains both the magnitude and the phase of the signal. When enough signal samples are recorded to k-space, it can be transformed to a magnetic resonance image by Fourier transformation. [44-47]

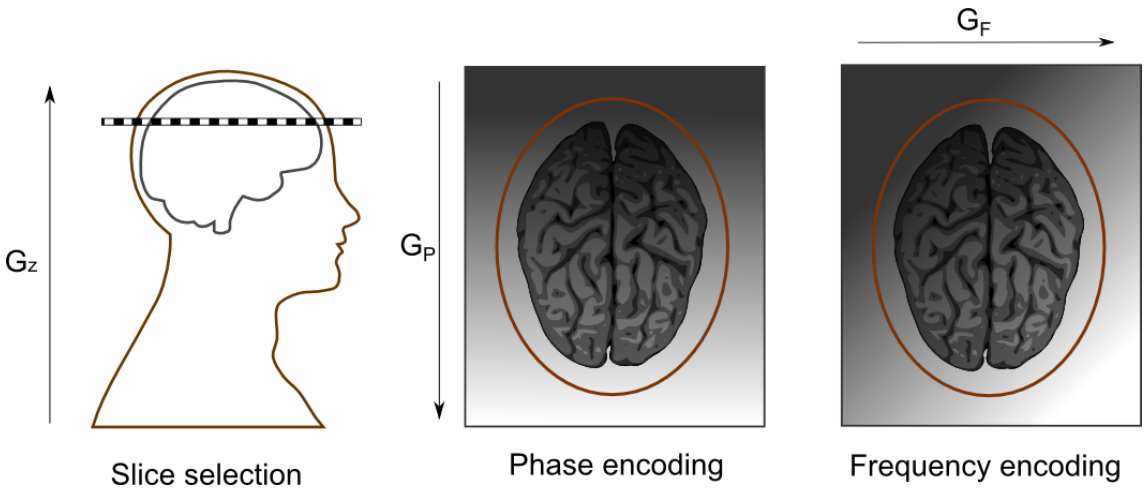

Figure 7. The role of each gradient in signal localization. The darkness of the background is representing the phase shift of the net magnetization in respective location.

2.1.4. Basic pulse sequences

The pulse sequence describes how radio frequency pulses and magnetic field gradients are arranged together to create desired echo signal. The pulse sequence is repeated periodically with a time interval called the repetition time T_R. Similarly, the time between initial RF pulse and the maximum echo strength is called the echo time T_E.

All of the pulse sequences are generally based on two base sequences called gradient and spin echoes. In gradient echo sequences the measured echo is generated by utilizing the gradients to produce a change in field strength and hence a corresponding change in Larmor frequency along a particular direction. When a magnetic field gradient is switched on it causes proton spins to lose coherence or dephase rapidly along the direction of the gradient as they precess at different frequencies. The amount of de-phasing caused by one magnetic field gradient can, however, be reversed by applying a second magnetic field gradient along the same direction with inverted magnitude. If the moment of the second gradient is the same as the first gradient, the de-phasing caused by the first gradient is cancelled. The gradient echo is following T2* relaxation since the gradient re-phasing cannot cancel out spin dephasing caused by the main magnetic field inhomogeneity. An example of the gradient echo pulse diagram is presented in Figure 8.

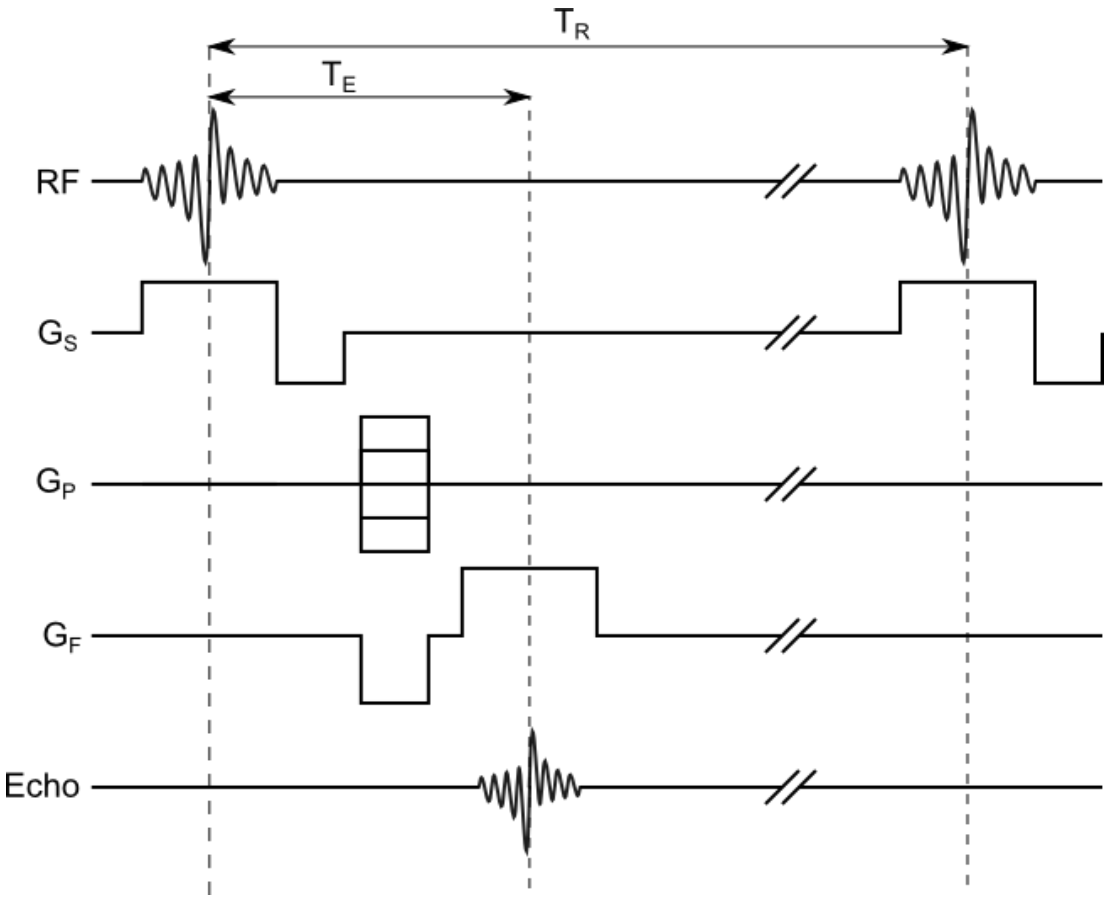

Figure 8. Gradient echo pulse diagram.

Spin echoes are generated by the application of a 180° refocusing RF pulse after excitation pulse. Unlike the gradient de-phasing in gradient echo sequences, the 180° refocusing pulse effectively removes the de-phasing caused by magnetic field inhomogeneities. Because of more effective re-phasing the spin echo is following the T_2, not T_2*, relaxation and the amplitude of the signal is greater than the gradient echo signal. The downside is that when the spins are not actively de- and re-phased, the TE times are growing larger than in the gradient echo sequence. [44-47]

2.1.5. Image artifacts

There are numerous possible artifacts that may compromise the quality of magnetic resonance images. Aliasing, ringing, motion, chemical shift and susceptibility artifacts are not specific for any particular application in MRI and are commonly encountered in clinical imaging. A collection of images representing the artifacts is presented in Figure 9. [48-51]

Image aliasing occurs if signal is received beyond chosen field of view (FOV) in phase encoding direction. The undesired signal is sampled to the k-space and transformed to image space along with the signal from the FOV. The result is an image where the unwanted parts of the image slice are wrapped over the desired image. Aliasing can be corrected by increasing the number of samples to cover the whole signal producing area or by nullifying the signal outside the desired FOV.

Gibbs or ringing artifact can be seen as bright and dark intensity changes in image borders with rapid intensity changes. The ringing follows from insufficient sampling of sharp intensity change. The lack of high frequency image frequencies is seen as bands of high and low intensity. The effect of ringing artifact can be reduced by increasing spatial encoding frequency.

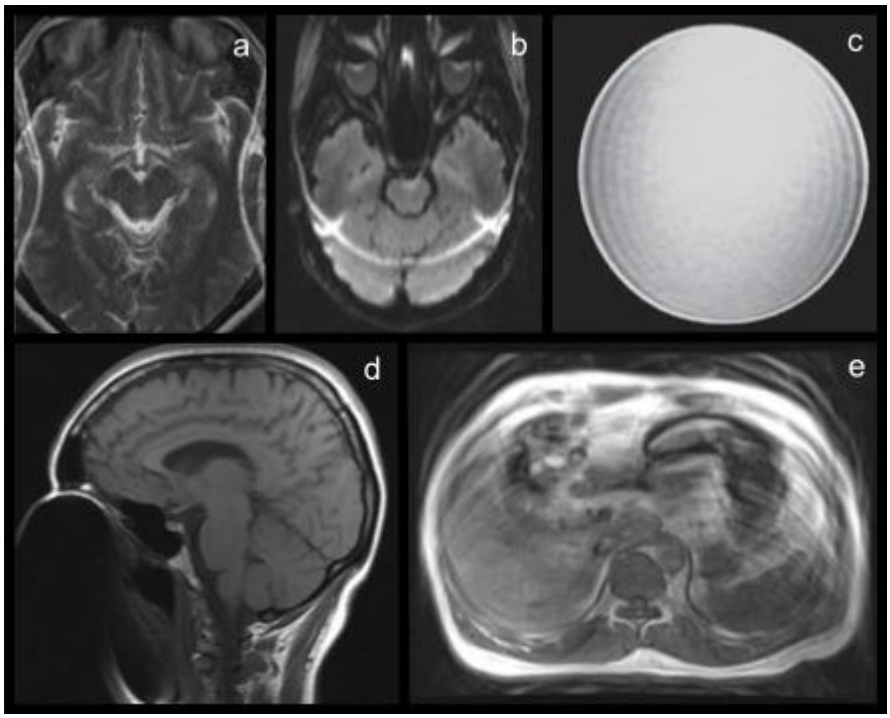

Figure 9. (a) Aliasing artifact, (b) chemical shift artifact, (c) ringing artifact, (d) susceptibility artifact caused by dental filling and (e) motion artifact caused by respiration. Adopted from [50].

The motion artifacts are resulting from undesired movement in target area during the imaging. If the location of the signal source is varied between the pulse repetitions, the image becomes ambiguous. The artifact is seen as blurring and ghost images in the

phase encoding direction. Often the cause of motion artifact is breathing motion and image quality can be improved by introducing breath hold imaging or respiratory gating as presented in Chapter 3.1.2.

Protons bound in water and fat molecules have different Larmor frequencies. The frequency difference is transformed in image reconstruction to spatial shift between fat and water in frequency encoding direction. The artifact is called chemical shift which amount is depending on the main magnetic field strength, pixel size and used RF receiving bandwidth. The effect of the artifact can be minimized by using large RF bandwidth or simply by suppressing the fat signal if it is not needed in the images.

All materials have a property called permeability which is a measure of material´s ability to support the formation of a magnetic field within itself. Basically higher the permeability of the material, stronger the magnetic field density in and around the object. The scanner can fine tune the main magnetic field to oppose the bending of the field at borders with subtle permeability changes. However, most metals have high permeability and susceptibility artifact is produced on and around the metallic object. The artifact is seen as signal void in the images because the distortion of the magnetic field is destroying the coherence of the spins and thus no signal can be detected from the area.

2.1.6. Hardware

The hardware of the MRI scanner is based on three different types of coils and electronics to drive them. The heart of the scanner is a superconducting coil generating the main magnetic field. The gradient fields, which are used to achieve signal localization, are formed with resistive gradient coils integrated in the scanner structure. RF coils are needed for transmitting and receiving the RF signal. Often, the transmission of the RF signal is done with a coil mounted in the scanner body whereas receiving is done with separate coil close to the area of interest. [52]

In the course of development of the MRI machines there has been drive to reach higher field strengths because it provides more signal as explained in Chapter 2.1.1. Ultimately, this leads to better SNR which then can be utilized for increased spatial and temporal resolution. Along with the main magnetic field, the frequency of transmitted

RF field has to increase respectively. With increased frequency the body absorbs the RF pulses more effectively and makes the even field strength distribution inside a body harder to achieve. This is leading to higher specific absorption rate (SAR) and variable magnetization tipping angles inside the FOV. [52, 53]

In order to achieve reasonable scanning speed, the switching of the gradient fields has to be rapid exposing the scanner hardware to eddy currents (Figure 10). Currently the speed of gradients are mainly restricted by the physiological limitations of the human body. [52, 54, 55]

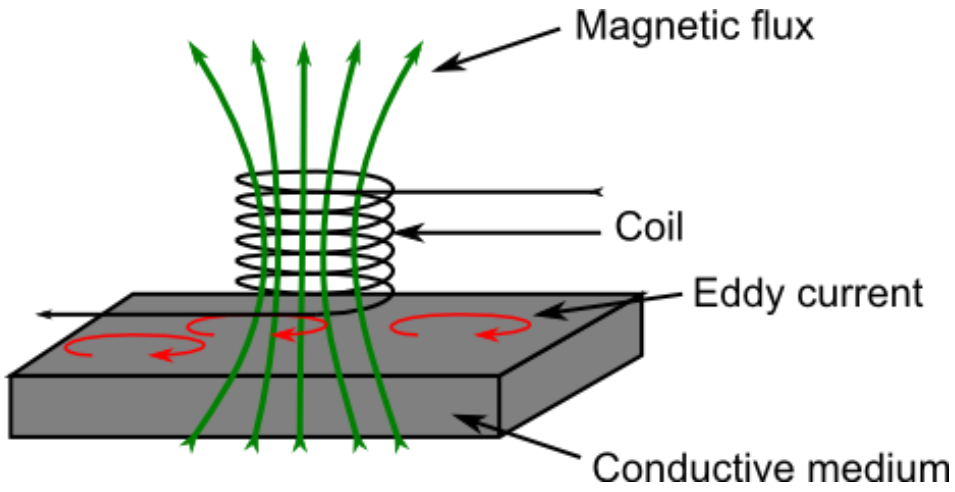

Figure 10. Illustration of the eddy current formation. Changing magnetic flux induces electric current in the conductive medium which is again producing new magnetic field.

RF signal receiving is done with special coils that are optimized according to the purpose of use. For example, the head coil is designed to give a good reception in head volume whereas the spine coil is optimized to record signal only from back and spine. Signal receiving can be done with multiple parallel coils if the sensitivity of each coil relative to other is known. The parallel imaging can be speed up scanning remarkably because the required signal for the image can be recorded faster. However, special reconstruction methods are needed. [56]

2.2. Phase contrast velocity encoded pulse sequence

In velocity encoded phase contrast pulse sequences, the velocity of the signal producing tissue is transferred in the phase information of the acquired signal. This transformation is normally based on the utilization of a bipolar gradient pulse in gradient echo imaging. The formation of the gradient echo requires rephasing of the spins. Normally, this is achieved by applying two gradients with identical moment apart from opposing polarities on frequency encoding direction, hence the name bipolar pulse. However, the strength of the magnetic field varies along the direction of the gradient so the phase of the magnetization returns to zero only if the source of the signal remains stationary. [57]

If the signal source has a velocity component along the direction of the gradient, it experiences the positive and negative gradient fields with different strengths and thus the phase of the magnetization is not completely reversed. Moreover, the remaining phase difference from the original is relative to the velocity of the source. Illustration of the phase travel is presented in Figure 11. If it is assumed that the there is no acceleration, the accumulated phase difference can be written with equation

$$\Phi(t) = \Upsilon v \int_0^t G(t) t \, dt \quad , \tag{7}$$

where Υ is the gyromagnetic ratio, v is the velocity of the signal source and $G(t)$ is the gradient [58]. From the equation, it is seen that by setting the shape and timing of the bipolar gradient pulse and measuring the resulting phase, the velocity of the signal source can be determined by solving the v.

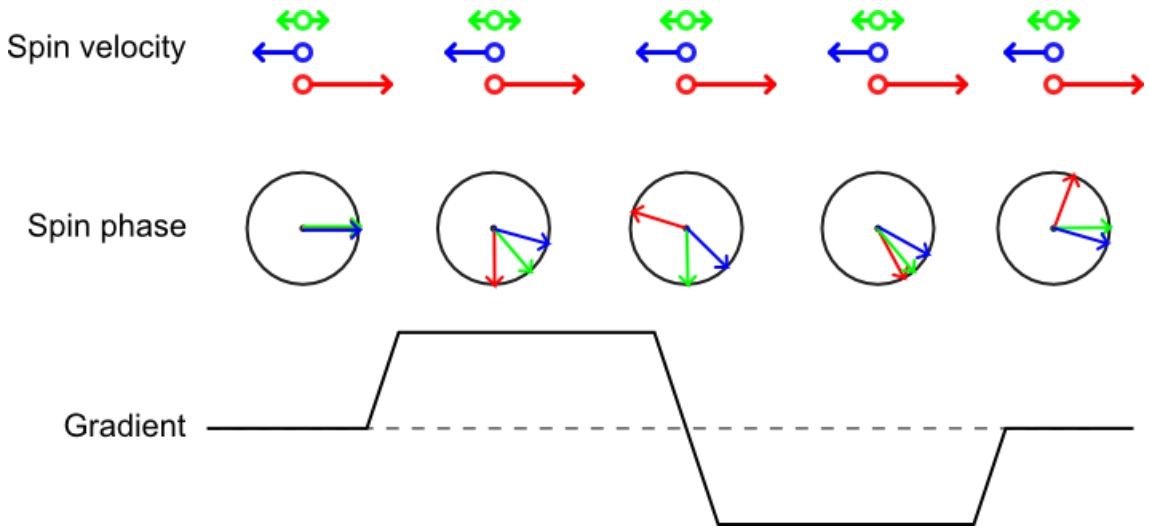

Figure 11. Illustration of spin phase development through the phase contrast velocity encoded sequence. The green spin is stationary, blue is moving slowly to the negative direction and the red is moving fast to the positive direction.

Phase image can be uniquely defined only within 2π range. Usually in the clinical imaging sequences the phase offset is set so that π is representing the maximum flow velocity that can be defined unambiguously and respectively -π is the same velocity magnitude with opposite direction. The maximum velocity that the sequence is able to handle is normally referred with the parameter V_{ENC}. In hardware terms the V_{ENC} parameter controls the moment of the velocity encoding gradient. The difference between the uniquely detectable maximum and minimum velocity is often referred as velocity window.

Not all phase changes are originating from the movement. For example, main magnetic field inhomogeneities and eddy currents among others are responsible for additional phase accumulations. In response to this, typically two acquisitions with different phase encoding gradients are used to minimize the unwanted effects. Most of the hardware error factors are ruled out from the results when these two signals are subtracted with exception of phase offset produced by velocity encoding gradient induced eddy currents.

After the reconstruction and subtraction, the phase of each voxel in the image represents the velocity in the direction of the applied bipolar gradient. Typically, the velocity map is presented as an image where mid-gray pixel represents the stationary tissue and white

and black pixels respectively maximum unambiguously measurable velocity in the positive and negative directions along the velocity encoding gradient.

2.3. Introduction to fluid mechanics

The fluid in motion follows two principal rules: Firstly, there are no velocity discontinuities in the flow. Secondly, there is no velocity discontinuity over the fluid-barrier border. This means that the fluid immediately attached to the wall of the fluid channel is stationary and there is relation between the flow speed and the distance from the wall.

The volume of blood remains relatively constant when the pressure is changing if volumes under study are large compared to the size of the blood cells. Thus blood can be considered as incompressible fluid especially when flow in large arteries are in question. Generally the blood flow can be described with the Navier-Stokes equation for incompressible fluid

$$\rho\left(\frac{\partial v}{\partial t} + v \cdot \nabla v\right) = -\nabla p + \mu \nabla^2 v + f \quad , \tag{8}$$

where ρ is the density of fluid, v is the speed of the fluid, p is the pressure of the fluid, the μ is the viscosity of the fluid and f represents other body forces such as gravity and centrifugal force. The equation tells that the density of fluid is a scaling factor for the flow.

The varying diameter of the blood vessels does have important effect on the flow. In vessels with similar wall material the speed of the flow is inversely depending to the diameter of the vessel squared. This means that if the diameter of the vessel is halved, the speed of the blood flow is quadrupled as presented in Figure 12. The acceleration of flow is giving a raise to more complex phenomenon called turbulence. [59]

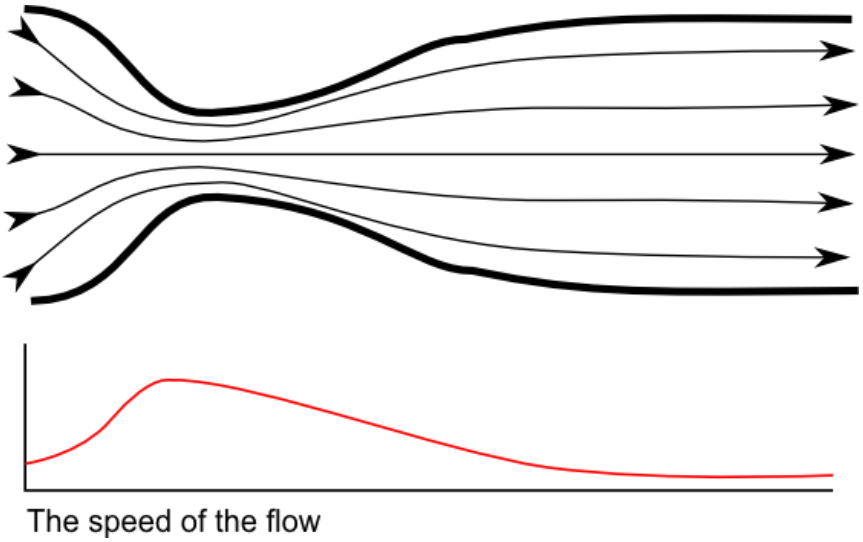

Figure 12. The speed of the flow relative to the location in the vessel with varying diameter.

Generally, turbulence can be described as a collection of vortexes resulting from mixing of fluids travelling with different speeds. The transition threshold between smooth laminar flow and violent turbulent flow is not always easily determined from flow characteristics. One commonly used parameter for describing the nature of a flow is called the Reynolds number which represents the relation of inertial forces to the viscosity of a fluid. The Reynolds number of flow can be calculated with an equation

$$Re = \frac{\rho D_L v}{\mu} \quad , \tag{9}$$

where ρ is the density of a fluid, D_L is the hydraulic diameter of a vessel, v is the velocity of the flow and μ is the viscosity of the fluid. The hydraulic diameter can be solved with equation

$$D_L = \frac{4A}{L} \quad , \tag{10}$$

where A is the cross-sectional area of the vessel and L is the circumference of the vessel. For the special case of a pipe with circular cross section the hydraulic diameter equals the diameter of the cross section.

There is no single value of Reynolds number that is dividing flow into laminar and turbulent. However, it is presented that with a circular pipe in steady conditions flows under Reynolds number 2300 are laminar and over 4000 turbulent. The mean Reynolds number of flow in blood vessels is normally in the region of 2000 indicating laminar flow. However, when stenosis is present in the vessel, possibly combined with pulsatile flow, Reynolds numbers may reach high values up to 5000 - 15000. [60-62]

2.4. Magnetohydrodynamic effect

The magnetohydrodynamic effect is created by conducting fluid moving in magnetic field. Blood is rich in ions making it an excellent conductor and a source of magnetohydrodynamic potentials. The amount of magnetohydrodynamic voltage produced can be described by equation

$$V = \int v \times B \, dL, \tag{11}$$

where B is the magnetic flux density, v is the velocity of the fluid, and L is the diameter of the vessel. The relation to the main magnetic field strength means that the effect is increasing in high magnetic fields. Also, the voltage is maximized when the direction of the magnetic field and the flow are perpendicular. Strong magnetohydrodynamic voltages are thus produced in the bends of large arteries where the speed and volume of the blood is also high. Such places in human body include especially aortic arch, as presented in Figure 13, and both the left and right pulmonary artery. [63, 64]

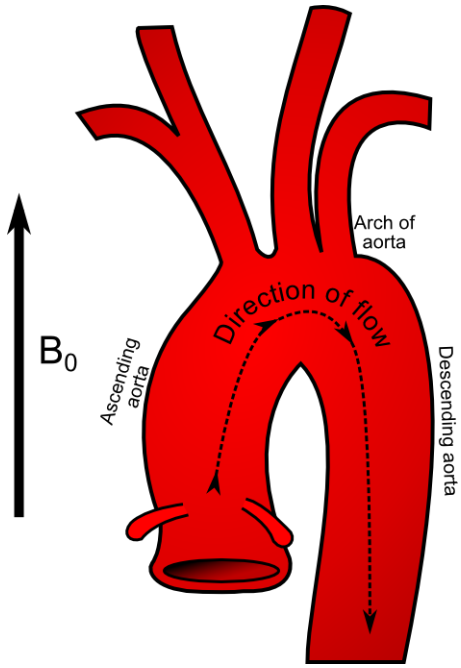

Figure 13. The direction of the flow in the aortic arch in respect of main magnetic field in typical imaging setup.

The electrical signal produced by the flowing arterial blood in the magnetic field is added to the electrical signal generated by the contracting ventricles since both phenomena are happening approximately simultaneously. This effect is especially important in respect of electrocardiography (ECG) signal recording in a magnetic field. Magnetohydrodynamic effect can be seen in ECG as higher T peak than expected. [65]

2.5. ECG gating

In order to study heart with the MRI, the whole imaging process has to be synchronized to the sinus rhythm of the heart. Usually this done with ECG gating using the electric potential changes around the heart during the pumping cycle. The largest peak in the ECG signal, the R-wave, is representing the contraction of the ventricles. An example of the ECG signal with respective peak labels are presented in Figure 14. The R-wave is typically set as the zero point of the heart cycle and all other time intervals are referenced to it. Other methods for cardiac gating are based on pulse oximeter or rarely on ultrasound [66]. Also, the whole gating process can be done retrospectively just by looking at the MRI data [67].

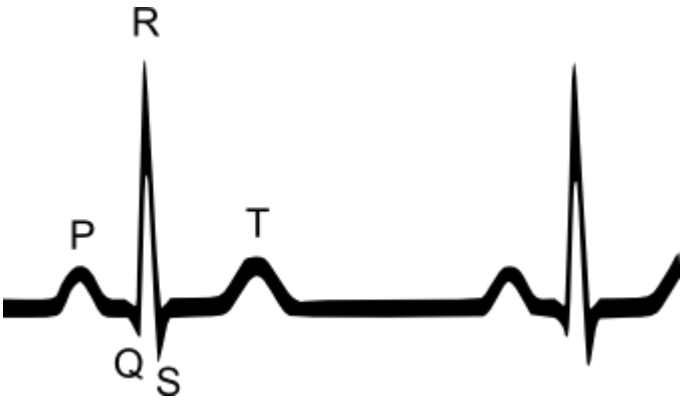

Figure 14. Illustration of the ECG signal. The peaks are marked with respective labels.

The time span of single heartbeat is too short to form a magnetic resonance image with good quality. ECG gating is used to set the imaging happen in the similar cardiac phase of every heart cycle. When it is known which phase of the cycle the data is related to, it is possible to generate an image of a single moment in heart cycle although the data is obtained during several different heart cycles. However, major arrhythmias may complicate the situation which is discussed in Chapter 3.2.5.

There are basically two cardiac gating methods in MRI to choose from: Prospective and retrospective gating. In the prospective gating the R-R interval of the heart is estimated beforehand. In the retrospective gating the scanner is imaging constantly and later the acquired data is sorted according to the recorded heart beats. Both methods have unique positive and negative aspects depending on the patient [68].

Instead of ECG, vectorcardiography (VCG) is often used for cardiac gating in MRI. In VGC the magnitude and the direction of the electric dipole of the heart is presented as a vector. The basic principle of the VCG is presented in Figure 15. The method is more robust in comparison with the ECG since the vector components can be filtered to minimize interference. VCG gating is important especially with high field strengths where the magnetohydrodynamic effect is strong. [69, 70]

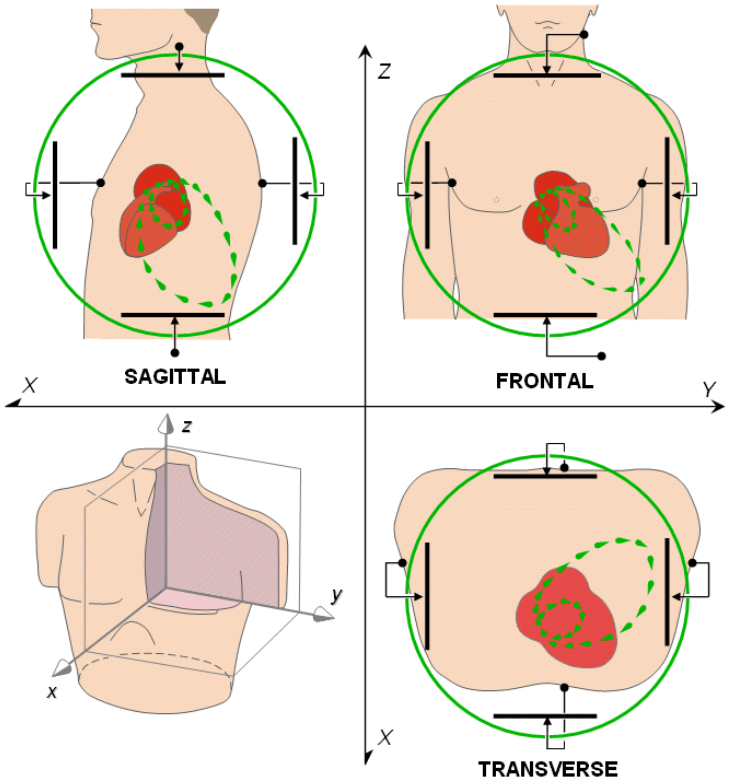

Figure 15. Illustration of the basic principle of vectorcardiography. The travel of heart´s electric vector is projected to the three orthogonal axes as presented with broken green line. Adopted from[71].

3. Review of error factors related to phase contrast velocity encoded measurements

3.1. Physiological error factors

3.1.1. Deformation of the heart

During systolic part of the cardiac cycle, the aortic valve is moving distal to the ventricle and the velocities of the moving aortic root and the arterial flow itself are added up. During the diastolic part of the cardiac cycle the amount of flow is damped when the aortic root is withdrawing back to its original position. The same happens also with regurgitant flow but in opposite order since the direction of the flow is reversed. It is reported that the extent of the cardiac movement during single heart cycle can be as large as 1 cm with speed up to 10 cm/s. [72]

The most commonly used method for reducing the error generated by moving heart structures is a careful positioning of the imaging plane. The optimal place for the plane is far enough distal from the valve to leave distinct clearance but also close enough to catch the laminar region of the flow. The optimal placement of the measurement plane is further discussed in Chapter 3.2.6 and studied in detail in Chapters 4-6.

Another way to take the deformation of the heart in to account is to sacrifice part of the imaging time to map anatomical landmarks. A special sequence can be used to detect the position of the heart valve through the imaging sequence. With the help of the anatomical navigator, the imaging slice can be positioned in respect to the position of the heart valve during each heart phase instead of fixed hardware coordinates. This method, called "Moving slice velocity mapping", is pioneered by Kozerke et al. [73]. However, moving slice velocity mapping is not yet available in commercial scanners.

3.1.2. Breathing motion

The heart´s position from one beat to another may change considerably due breathing motion. Various methods from different breath holding techniques to sophisticated signal processing methods have been presented to avoid breathing motion related error. The easiest way to handle the breathing problem is to not care it at all and tolerate the

results. If the images are put together from data collected during several R-R intervals, as in cine sequences for example, the images are likely to become blurred. It is also important to remember that if a stack of images is obtained without any corrective measures, the consecutive slices are not necessary anatomically aligned. The image quality in free-breathing imaging can be substantially improved if data averaging is used. Especially with arrhythmic or very ill patient it might be the case that free-breathing imaging may be the most effective way to do cardiac imaging. [74]

If the quality of images needs to be improved, breathing movement has to be taken account. The most straightforward method to achieve this is to request the patient to stop breathing for a short period of time. Usually a 10-20 s breath-hold can be achieved. Typically, this is long enough to scan a few slices of cine images. As in free-breathing imaging, it has to be remembered that the position of the heart varies between the successive breath-holds and thus the anatomical alignment of the structures may be compromised.

There is also another error source in breath hold imaging: The physiological parameters of flow are different during free-breathing and breath-hold. The amount of error is studied by several groups with similar results [75-77]. It is found that the breath-holding is reducing the amount of flow measured by phase contrast flow imaging compared with free-breathing. However, if the patient is instructed to hold breath after expiration the error is found to be in order of a few percents. With inspiratory breath-hold error up to 25% may be present [76].

Free-breathing imaging suffers from compromised image quality and breath-hold imaging requires good cooperation of the patient which is not achieved in many cases. Due to these difficulties, various technical methods are presented to decrease the effect of breathing motion. Probably the most straightforward solution to monitor the breathing cycle in the MRI is the use of a respiratory belt. In this method a special belt is placed around patient´s abdomen which is sensing the movement of the abdominal wall. With the information of the abdominal wall position, the imaging can be set to occur at desired part of the breathing cycle. This method has been found to improve the image quality considerably compared to free breathing studies. However, there is a risk that the belt becomes dislocated during the imaging process and thus interrupts the

whole study. Additionally, the method requires extra hardware to be present inside the scanner with the possibility of susceptibility artifacts. [78]

The most effective technical solution to control breathing motion related artifacts is the use of navigator pulse. Typically the position of the diaphragm is mapped with a one dimensional navigator pulse which is blended in the actual imaging sequence. The resulting navigator image is consisting of a grayscale bar which can be used to detect the lung-diaphragm border through the imaging sequence. Typical positioning of the navigator is through the diaphragm as presented in Figure 16. After the analysation of the navigator data the breathing pattern for the length of imaging sequence is obtained and can be used to correct movement artifact in the actual imaging data [79, 80]. In addition to actual navigator position, an acceptance window has to be chosen. The acceptance window determines how much the diaphragm can move without imaging data to be discarded as presented in Figure 16. If too small value is chosen, the images are sharp, but only a small part of the breathing cycle is used for imaging and the scan duration may become inconveniently long. When using navigator correction, it is always good to remember that the time used be the navigator pulse is away from the actual imaging pulse which is lowering the efficiency of the imaging sequence, especially if there is a navigator pulse included in every excitation cycle of the actual imaging sequence [81].

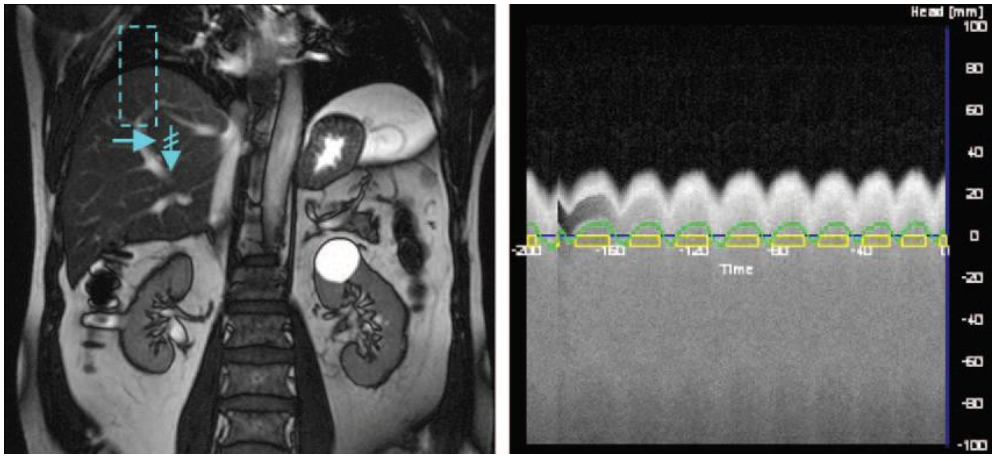

Figure 16. Presentation of navigator position and acceptance window during typical breathing pattern. Navigator is marked as light blue in the left image. Yellow boxes in the right image are representing diaphragm positions which are inside the acceptance window. Adopted from [51].

3.1.3. Valve defects

Cardiac valves are shaping the flow downstream from the valve as the function of the pressure difference over the valve. In case of normal aortic and pulmonary tract the valve opens fully and provides relatively free passage of the blood towards the arteries. However, if the valve becomes dysfunctional, it will effect strongly on the speed and complexity of the velocity field downstream from the valve and produce error to the velocity encoded flow studies as presented in Figure 17 [19, 82].

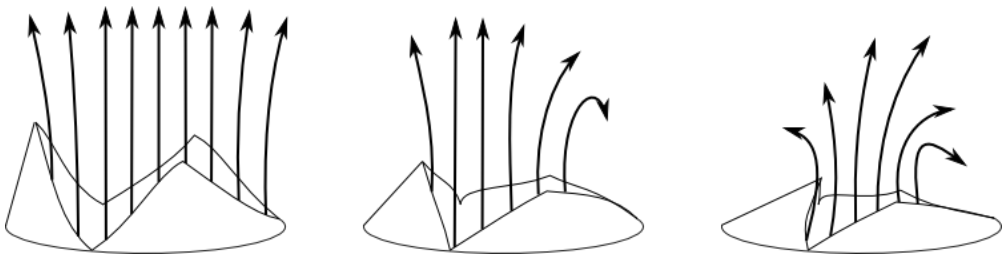

Figure 17. Flow patterns related to degrading of the heart valve.

Typically dysfunctionality, and ultimately stenosis, of the valve involves calcification [83]. Probability of calcified heart valves becomes significant typically with patients in the sixth decade of life or older. In addition to age, other risk factors include male gender, smoking and elevated cholesterol levels. Additionally, a few percent of population is carrying an aortic valve with only two leaves instead of three which is increasing the risk of valve calcifying in even younger age due increased turbulent flow [84]. Additionally, there are many congenital heart diseases that effect on the functionality of the valves and therefore produce complex flow patterns.

In a dysfunctional valve the movement of the leaflets is limited which is increasing pressure inside the ventricle. The speed of the flow is depending on both pressure gradient and the cross-sectional area of the passage. If the speed of the flow increases, it is inevitable that also the Reynolds number of the flow is increasing. At some point a speed is reached where the nature of flow is changing towards more chaotic behavior. In addition to pure speed, the exact form of the degenerated valve orifice is effecting strongly to the shape of the jet [85].

If the valve degeneration proceeds to a critical stage, it is changed to an artificial model. Currently there are two types on valve replacements: The classical type is a mechanical

valve which is consisting from a one-way port attached to an anchoring structure. The construction is found to be very durable but it has some flaws. Due to turbulent flow behavior near valve components, some blood clotting may occur exposing patient to extensive anti-coalugant therapy. There is also some regurgitant flow through the mechanical valve closure. More recent approach to valve replacements is to use a bioprosthetic valve which is essentially a pig heart valve fitted to a suitable structure. Bioprosthetic valves are behaving almost like original ones in terms of flow, but are typically having life span of only 10-12 years. In respect of flow imaging, the problem in artificial valves is that each model has to be treated as individual. Every model, especially mechanical ones, have some degree of turbulent processes involved in normal forward flow as well as leakage. A gallery of different artificial valve types is presented in Figure 18. [86]

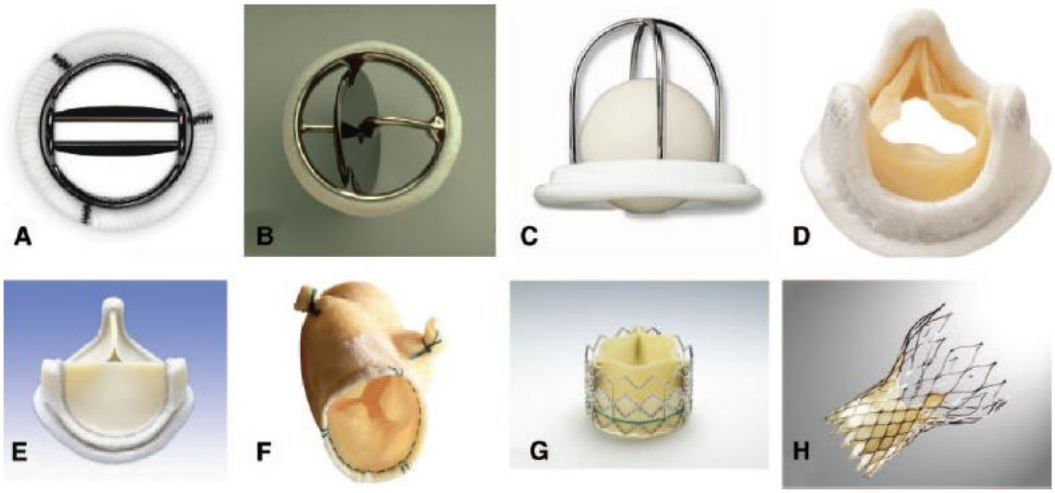

Figure 18. Different types of prosthetic valves. A, Bileaflet mechanical valve; B, monoleaflet mechanical valve; C, caged ball valve; D, stented porcine bioprosthesis; E, stented pericardial bioprosthesis; F, stentless porcine bioprosthesis; G, percutaneous bioprosthesis expanded over a balloon; H, self-expandable percutaneous bioprosthesis. Image adopted from [87].

Also, artificial valves are typically producing susceptibility artifacts. The most of the artificial heart valves are made from materials with low permeability and the artifact does not extend beyond the implant itself [88]. In addition to artificial valves, the susceptibility artifact of certain aortic stents may render all images from the thoracic area unusable [89].

3.2. Physical error factors

3.2.1. Phase aliasing

If the fluid velocity in the vessel of interest is exceeding the set velocity window, aliasing occurs. This is a common situation in clinical imaging when a cardiovascular disease is producing jets with high velocities up to 500 cm/s. Aliased signal phase is wrapped over the velocity window and the peak velocities are detected with opposite direction. An example of a phase wrap can be seen in Figure 19. Optimal selection of the parameter V_{ENC} is important because a too low value causes aliasing but too high leads to insufficient sensitivity.

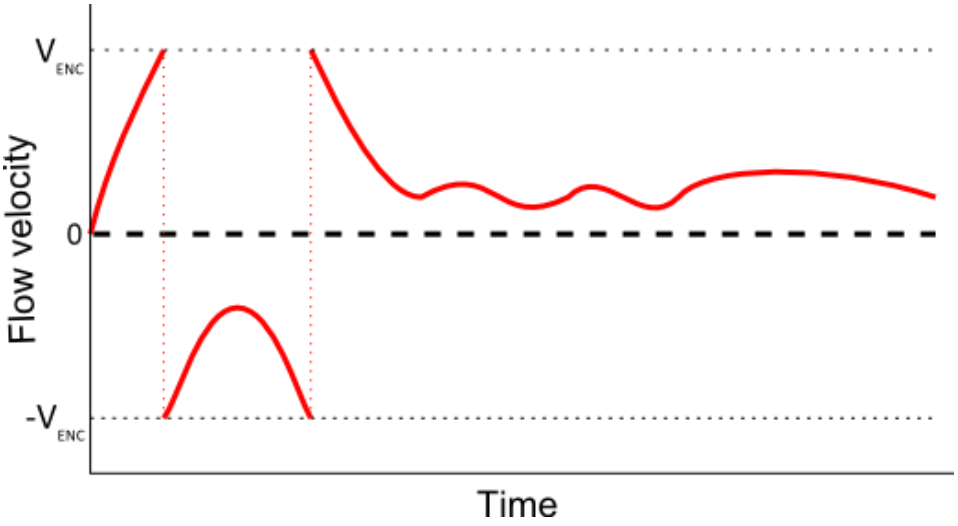

Figure 19. Example of an aliased flow plot.

Numerous methods for overcoming the aliasing problem have been presented. The most straightforward method is the use of baseline correction based on prior knowledge of the measured flow. For example, if the flow direction is not changing over time, image phase can be mapped as such that $-\pi$ is representing stationary flow and π maximum flow speed. Now in fact the velocity window has been fitted to match flow criteria and the extended range can be used to avoid aliasing and increase sensitivity. Also, a method where the parameter V_{ENC} is varied through the heart cycle to match the maximum flow velocity in each phase of the heart cycle has been presented [90]. There are also methods that can be utilized to unwrap an aliased image. Often these methods are based on the detection of magnitude differences in adjacent voxels coupled with statistical processing as in Guang et al. [91].

3.2.2. Partial volume artifacts

Phase contrast flow volume measurement is in principle an integration spatially over the voxel volume and temporally over the duration of the flow encoding gradient. This means that the voxels, which consist only partly of the desired flow medium, are averaged to mean flow velocity inside the voxel. Usually this happens at the lumen border where the voxels contain both stationary tissue and flowing blood. Example of the situation is presented in the Figure 20.

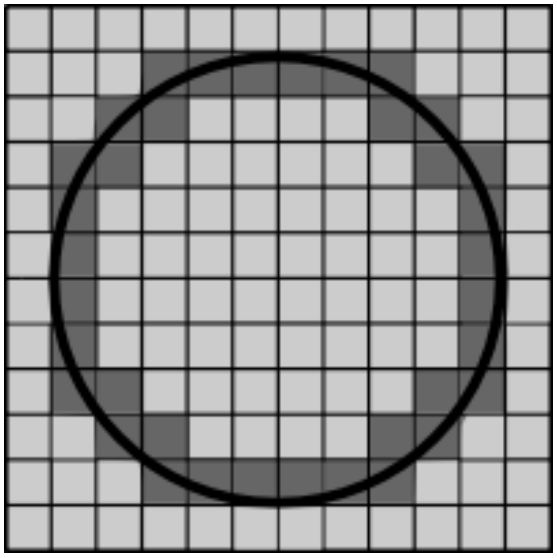

Figure 20. Cross section of a round lumen where flow velocity is measured. Partial volume artifact is experienced in the voxels which are marked with darker shade of gray.

It is presented that the measurement error of 10% or less is achieved if at least 3 voxels are covering the lumen diameter [92-94]. This is normally not a limiting factor when major arteries are imaged with modern MRI scanners, but might become a major issue if narrow vessels such as coronary or carotid arteries are studied. Also, if narrow high speed jets are present, problems may evolve. The flow velocity at the core of the jet may exceed the velocity of surrounding medium by multiple folds while being so narrow that the rule of three voxels is not satisfied. This is leading to at least slight underestimation of the peak flow speed in case of narrow jets.

3.2.3. Intravoxel dephasing

In addition to being integration over volume, phase contrast flow measurement is integration over the duration of the flow encoding gradient. This means that completely accurate results are only received from the spins that travel in straight line with constant speed. If a single voxel contains particles with varying speeds, also the spectrum of phase offset is broad and the resulting net phase of the voxel is an average of all phase vectors as presented in the Figure 21 [95].

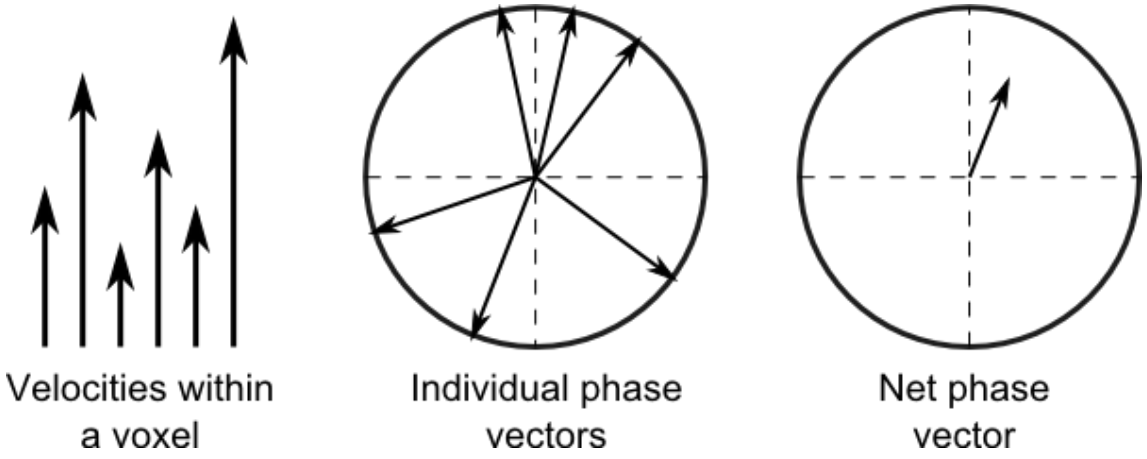

Figure 21. Phase averaging within a voxel containing particles with multiple velocities

This limitation has significance when turbulent flow patterns are imaged. Blood flow in the arteries is normally considered as laminar. However, several cardiovascular diseases are known to produce turbulent flow patterns and spatial variation in flow velocity. If the travel path of the spin is alternating from the straight line, the measured velocity is underestimated. This is because the final spin phase is related to the distance travelled in the flow encoding direction, not the total distance travelled. Examples of possible spin paths within a voxel are presented in Figure 22.

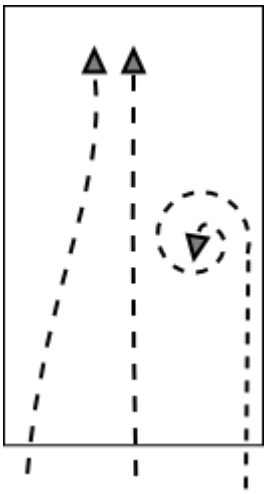

Figure 22. Possible spin population travel paths within a voxel.

Methods to completely cancel out the effect of intravoxel dephasing do not exist. The most straightforward method is to reduce the size of the imaging voxel [96]. Also, 4D phase contrast flow imaging can be used but still straight paths are assumed. In addition to the reduction of effects caused by turbulent fluid motion, it is equally important to be able to detect its existence. Efforts to quantify the amount of turbulence within a voxel have been made by Dyverfeld et al [20]. Simulation of the turbulent flow is also used to provide additional information on the magnitude of error caused by intravoxel dephasing in different setups [97].

3.2.4. Acceleration artifact

The technique used in the velocity encoded phase contrast imaging is only accurate with non-accelerating motion. This restriction is originating from the sequence design with a simple bipolar velocity encoding gradient. If the imaging plane is close to a region of accelerating flow, an error is produced to the measured flow velocities. Also, equation 7 is no longer valid since the velocity cannot be considered constant any more but as a function of time. If accelerating flow is imaged, the measured velocity is the mean of all velocities in the voxel over the duration of the velocity encoding gradient. Hence, the speed of accelerating flow is underestimated and decelerating flow overestimated. [12, 31, 98, 99]

In hydrodynamics the acceleration of the flow normally occurs when the cross section of the vessel is changing. As presented in Chapter 2.3., the speed of the flow is

inversely proportional to the vessel cross section squared. This means that rapid changes in a vessel diameter are leading to strong acceleration in flow (Figure 23). In the cardiovascular system such rapid changes in cross section are present, for example, in the vicinity of cardiac valves, especially if the valve is stenotic. In the stenotic cases relatively steady blood flow in the ventricle may transform to a narrow jet with flow speed up to 500 cm/s. If the measurement plane is overlapping with the decelerating flow, the measured flow speed is underestimated. To minimize errors, it is recommendable to place the measurement plane in the section of the vessel where the vessel diameter stays constant. Also, the minimization of the TE time of the sequence can be used to limit the amount of error as presented in Chapter 3.2.8. The optimal position for the measurement plane is discussed in Chapters 3.2.6. and 4-6.

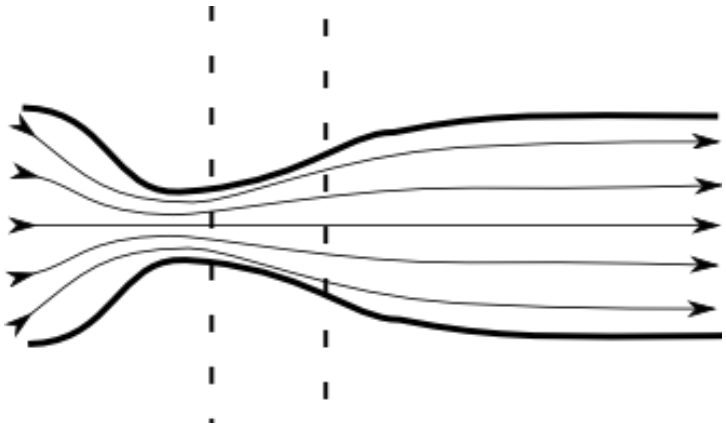

Figure 23. Flow accelerates if a narrowing is encountered in flow tract. Measurement error would be present in the slice position marked with broken lines.

In a recently published study by Barker et al. a sequence designed to image the acceleration of the flow was presented [100]. In the work acceleration encoded images were obtained directly by the utilization of specialized flow encoding gradients. The images were proven to be helpful in assessing abnormalities in the flow and visualize complex flow patterns.

3.2.5. Error sources related to cardiac gating

Prospective gating requires the operator to assign expected R-R interval before the imaging starts. When the R wave is detected, the scanner takes image frames for the duration of the set interval. In practice, somewhat shorter interval than the actual R-R time has to be chosen to avoid overlap with the next R wave. This is also the biggest weakness of the prospective gating because the last part of the heart cycle before the next R wave is not detected. On the other hand, prospective gating is robust. Normally major imaging artifacts caused by arrhythmias can be ignored because imaging is always started at the same phase of the heart cycle. This can be enforced even more by assigning arrhythmia rejection periods in relative to the R-wave where possible miss triggering is ignored. The schema of prospective gating is presented in Figure 24.

Retrospective gating can be described as an automatic method. It enables constant imaging with simultaneous ECG recording without online synchronization. Imaging is continued until required amount of data is collected. After the collection, the data is sorted according to the ECG into bins with desired duration. These data bins are then reconstructed individually to images representing respective heart phase. An example of retrospective gating is presented in Figure 24. In case of normal ECG, top quality flow image series are achieved. However, if the length of the R-R interval is changing radically from beat to beat or arrhythmias are involved, major artifacts may follow. This is because the sorting algorithm no longer knows which parts of the data are linked if the location of the R-wave becomes ambiguous.

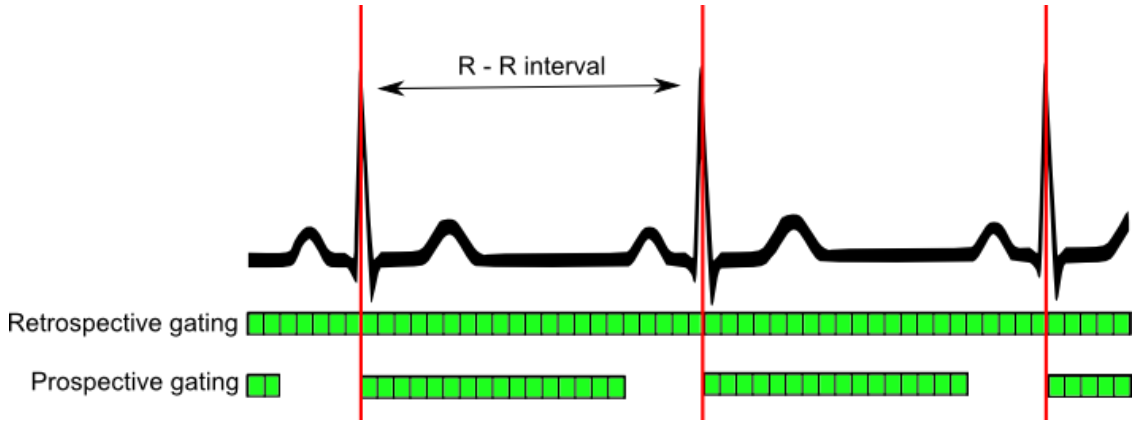

Figure 24. Retrospective and prospective gating. Image frames marked with green squares.

3.2.6. Slice position

Position of the imaging slice can have a strong impact on the flow measurements [26]. Some physiological factors, such as the amount of regurgitant flow, are best measured from different imaging slice location than the peak forward flow velocity for example. The importance of correct slice positioning is strongly related to the speed of the flow, which is further discussed in Chapters 4-6. With normal morphology and normal flow velocities it is not likely that slice position induced measurement error is going to have effect on the analysis. However, with highly accelerated flow there are complex processes which are varying along the direction of propagation and thus making good slice positioning invaluable.

Theoretically there are unlimited number of possible slice positions to choose from. Aorta is used here as an example vessel of interest to discuss about four measurement planes which are representing respectfully four different flow environments. These environments are immediately before and after the aortic valve, at the sinotubular junction and in the ascending aorta. The graphical representation of the planes can be seen in Figure 25.

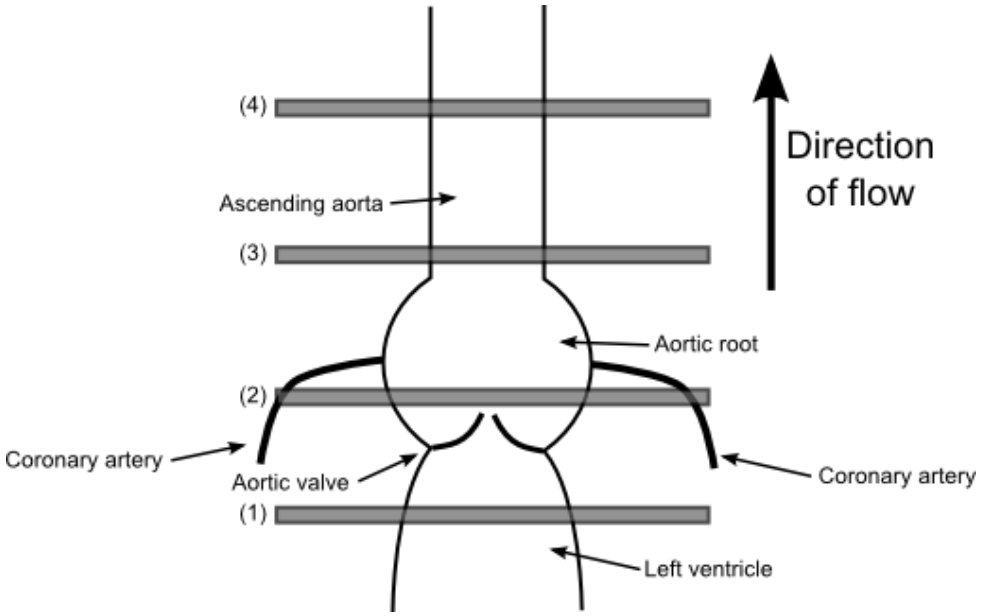

Figure 25. The model of the left ventricular outflow tract. Four example slice positions are shown: Just before the aortic valve (1), immediately after the aortic valve (2), at the sinotubular junction (3) and in the ascending aorta (4).

The measurement plane immediately before the aortic valve has many negative features. The diameter of a ventricle is normally narrow progressively towards to the valve so the nature of the flow is accelerating during the systole and thus making phase contrast flow measurement method inaccurate [101]. Ventricles are also moving during the heart cycle which may induce flows which are not contributing to the cardiac output. Nonelethess, the plane just before the aortic valve is a viable location to measure regurgitant flow [16].

When considering cardiac output, the measurement plane just after the aortic valve is physiologically the most relevant. This is because all the blood from the ventricle accounted in the net blood flow has to pass this plane. From the technical side, there are challenges. The first one is the movement of the aortic valve during the heart cycle. The movement of the valve may extend even up to 1.2 cm and reach velocities that are able to produce offset to the velocity encoded images [72]. Also, moving leaves of the valve can produce major artifacts to the phase images. There are a few papers which are describing sequences with variable measurement planes to solve this problem [72, 73]. In these sequences aortic valve is mapped throughout the heart cycle and the location of the measurement plane is defined by the distance from the valve. Another problem involved in the close proximity of the valve is the acceleration artifact. With modest flow speeds there is no significant deceleration present. Some heart diseases are however connected with stenotic dysfunction of the valve which may produce jets with speed up to 500 cm/s. After the high speed jet has passed the valve, rapid deceleration occurs and produces acceleration artifact to the measurements. The acceleration artifact is discussed in Chapter 3.2.4.

The easiest way to reduce the acceleration artifact is to move the measurement plane further to the downstream from the valve. The next interesting measurement plane is at the sinotubular junction. In most cases the flow in this region is relatively laminar and the acceleration artifact is producing only minor error even in the stenotic case. However, coronary arteries are originating upstream from the sinotubular junction and thus coronary blood flow is absent from the measurements performed at this level. The percentual amount of the coronal flow out of the total cardiac output is varying from person to person, producing a small yet unpredictable error to the flow results. [59]

It is also a considerable option to place the measurement plane all the way up to the ascending aorta. The diameter of the ascending aorta is relatively constant although there are some temporal variations due to pulsatile nature of blood flow. The acceleration artifact is thus minimized and the flow is theoretically very laminar. However, jets originating from stenotic heart valves may extend all the way to the ascending aorta and produce turbulent flow. Also, if there is any regurgitant flow present at the valve, it is unlikely that it can be seen in the ascending aorta. This is because the blood volume involved in the regurgitant volume is reserved in the enlarged aortic root during the systolic phase. Additionally, as in the measurement plane at the sinotubular junction, coronary blood flow is absent from the measurements made in the ascending aorta. [59]

3.2.7. Slice alignment

In clinical use, the flow is usually encoded in one direction. In case of diverting flow and encoding vectors, the speed of the flow is underestimated by a factor of $\cos \alpha$, where α represents the angle between the flow velocity and the flow encoding direction. Also, the encoding direction and the flow velocity vector may be aligned, but the measurement plane is not perpendicular to the vessel of interest. In this case the cross-sectional area of lumen is misregistered oversize by a factor of $1/\cos \alpha$. Enlargement of the lumen as a funtion of α is visualized in Figure 26. [102]

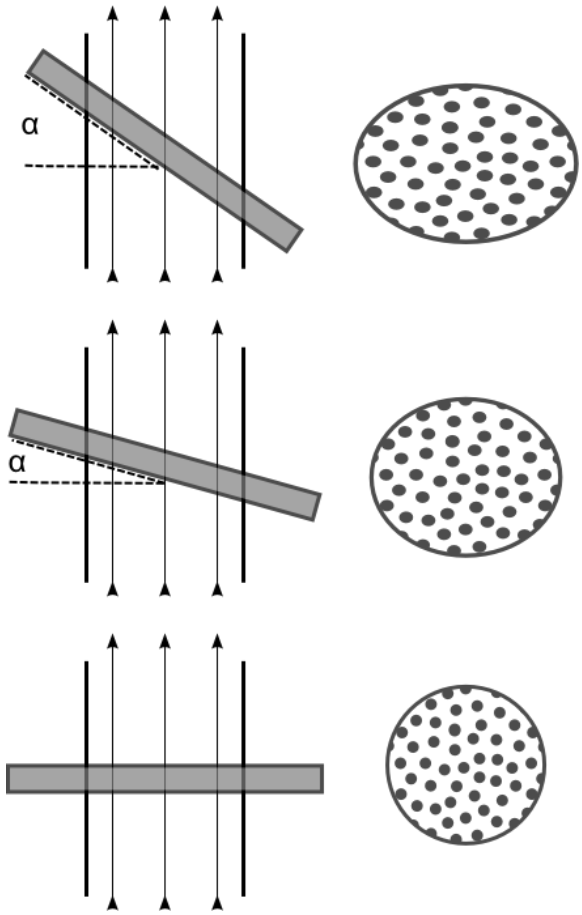

Figure 26. Example slice alignments on the left and corresponding flow lumens on the right.

In the currently used commercial scanners the flow encoding direction is usually set to be perpendicular to the scan plane to avoid problems with measurements. In this particular situation flow encoding direction misalignment and oblique scan plane are effectively cancelling each other out [102]. However, the underestimation of the peak flow velocity is still present and has to be taken into account.

Also, in the case of stenotic flow there might be one or more jets present within a flow. The jet may alter from both the direction of the vessel and the general flow direction in the vicinity. In these cases it is impossible to completely avoid misalignment errors. However, it advisable to optimize the measurement according to the jet to catch the peak velocity of the flow.

3.2.8. The effect of TE time

The measured velocity in a single voxel is integrated over the duration of the velocity encoding gradient. In commercial scanners it is difficult to find out the actual length of the velocity encoding gradient. However, it has to be shorter than the TE time of the sequence and most likely closely depending on the TE time as well. [96]

The effect of TE time was extensively studied by O´Brien et al [58, 96, 103]. The group suggested that the principal method of decreasing the error in velocity encoded flow measurements would be to lower the TE as low as possible. With minimum TE time, the effect of turbulent processes in the flow and irregularities of the hardware would be minimized. In their in vitro work O´Brien et al. studied how MRI phase contrast sequences with different TE times succeeded in the measurement of flow volume in stenotic setup. It was demonstrated that the measured flow volume was significantly underestimated even at the moderate speed of 300 cm/s with TE of 4.8 ms whereas the measurement was relatively error free with flow velocities up to 500 cm/s when TE of 2 ms was used. In their later in vivo study the group used an ultra short TE sequence (UTE) with only 0.65 ms TE and compared the results with a more conventional phase contrast sequence with TE of 2.85 ms. It was noted that the UTE was able to record consistent velocity profiles in the human aorta independent of the slice position distance to the valve whereas the variation in results between the measurement positions were considerably higher in the sequence with longer TE time.

In commercial scanners it is normally not possible to achieve TE times much less than 2 ms in phase contrast sequences and even in the experimental setups 0.65 ms mentioned above is the current state of art. The problem with the very low TEs is that the slew rate of the gradients has to be very high. This itself is also a factor that is limiting the minimum achievable TE, but before everything, it is giving a raise to excessive phase errors originating from eddy currents [96]. Eddy currents related artifacts are discussed in Chapter 3.2.10.

3.2.9. Temporal resolution

When flow volume through a chosen surface during one heart cycle is measured, the duration of the cycle is divided into a number of image frames. The optimal number of image frames chosen for a sequence is essentially limited by two factors: velocity averaging and signal to noise ratio (SNR). If the number of image frames is set very high, less signal is used to form a velocity encoded phase image and thus SNR is decreasing. On the other hand, if a very low number of image frames is used, velocity averaging occurs.

The effect of the number of image frames was studied by Garcia et al [104]. They presented that only small changes in measured flow volume was seen if at least 24 image frames were used. Even with 16 image frames deviation is within tolerable limits. The effect of the number of used image frames on the measured flow volume can be seen in Figure 27. However, it has to be kept in mind that in case of exceptionally fast flow the averaging of the flow becomes more important issue and number of image frames has to be increased.

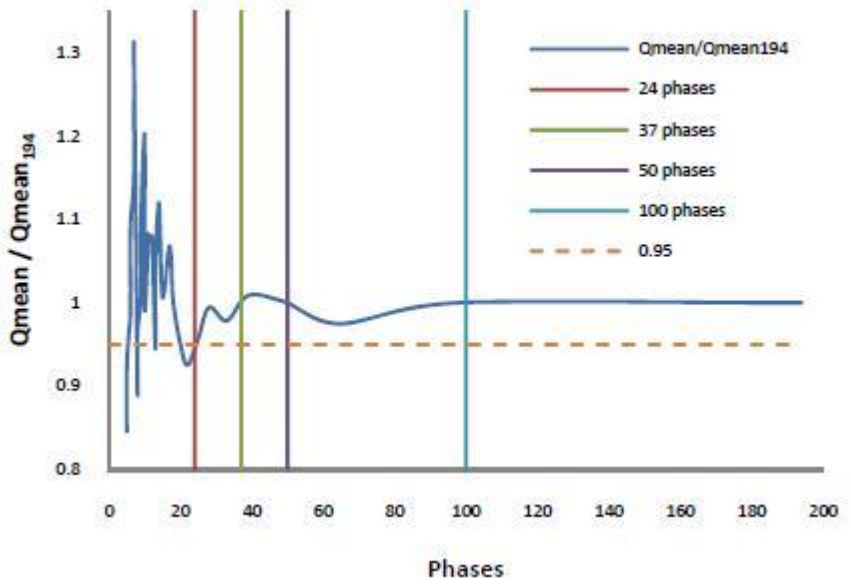

Figure 27. The relative measured flow volume compared to the flow volume measured with 194 image frames (phases) per heart cycle[104].

3.2.10. Eddy currents

Whereas in standard image reconstruction phase offset of a few degrees do not notably affect image quality, in phase contrast flow imaging it is directly transferred to velocity offset. A recent study Gatehouse et al. pointed out that currently there is velocity offset incorporated in images obtained with all commercial scanners produced by three different manufacturers [105]. Mostly this is a problem the hardware producers are constantly battling against but there are also some error reducing methods that can be applied by the user.

Practically all offset producing eddy currents are produced by the velocity encoding gradient since the actual phase image is formed by subtracting two images with identical settings apart from the gradient. The strength of the produced eddy currents can be lowered by decreasing the slew rate of the gradients. However, TE time is respectively increased to undesired levels if the slew rate is lowered too much. The amount of phase offset produced by eddy currents is practically impossible to predict beforehand. In a recent study the effect of several imaging parameters on phase offset was studied by Rolf et al. who found no major link applicable to all scanners [106].

Currently two methods are used to correct eddy current induced phase offsets. The first one uses phase of a known stationary tissue adjacent to the vessel of interest. The phase of all voxels in the image is corrected by the angle measured in the stationary tissue. However, usually there is no guaranteed stationary tissue immediately next to the desired area and neither is the phase offset constant over the image [107]. The other correction method is based on the utilization of a stationary phantom. The phantom is placed in the scanner immediately after the patient and the sequence is run again with exactly same slice position and parameters [108-110]. The phantom image is used as a correction map which can be applied to the patient image. Results achieved with the method are rather impressive as presented in Figure 28.

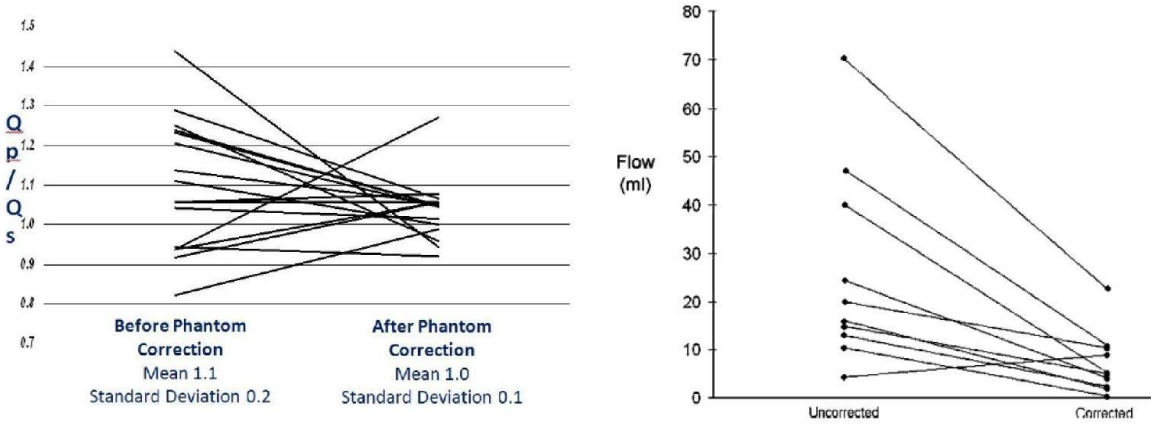

Figure 28. Effect of the phantom correction method on the flow volume ratio of the pulmonar and systolic flow. Relative results presented by Holland et al. [110] on the left and absolute result produced by Chernobelsky et al. [108] on the right.

3.2.11. Chemical shift artifact

Chemical shift has not been considered having major impact on phase contrast flow encoded imaging in the past. However, in a recent paper Middione et al. presented that over 5% error can be produced to the results if perivascular fat is present [111]. The error was generated when there was a layer of perivascular fat around the blood vessel and the imaging sequence had a narrow bandwidth. In that case, the stationary fat signal may shift inside of the vessel lumen as presented in Figure 29.

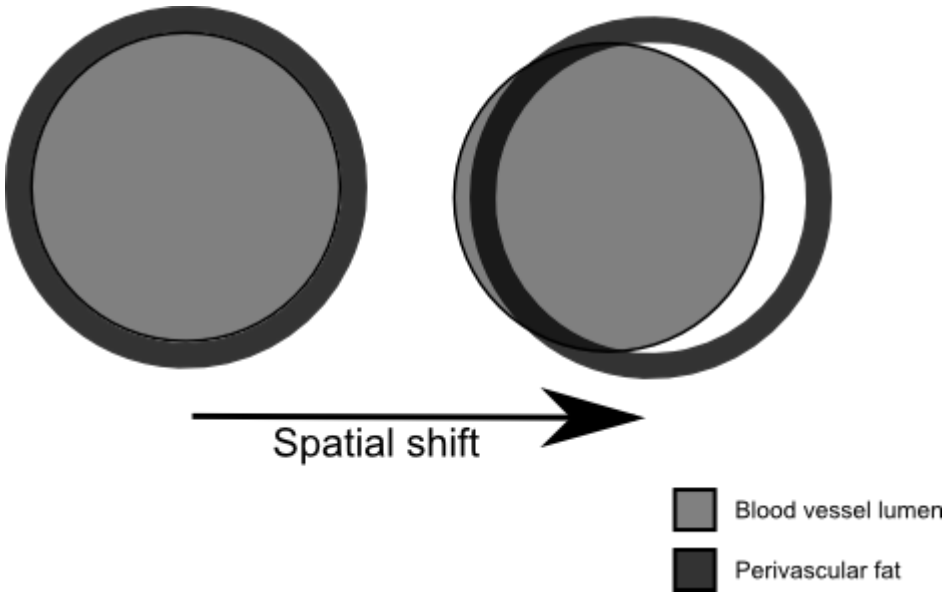

Figure 29. The chemical shift of the perivascular fat.

In their study Middione et al. show that the amount of chemical shift artifact is depending on bandwidth and TE time of the used imaging sequence. For example, in volunteers with pericardial fat, the mean difference in net forward volume was 6.4 ml between the least and most error prone sequence used. The presented methods to reduce chemical shift artifact does include the use of high RF bandwidth and sophisticated selection of the TE time. In respect of TE time selection, it is shown that minimum amount of chemical shift error is produced when the fat and blood signals are in phase. However, this conflicts with the assumption that the minimum error is achieved with minimum TE.

When the diameter of the vessel in interest is exceptionally small compared with amount of perivascular fat involved, it might be advisable to take special measures to limit the amount of chemical shift artifact. With minor amount of perivascular fat and major arteries it is likely that efforts to reduce chemical shift artifact may generate more problems than solve.

4. Effect of slice location on measured flow volume: Materials and methods

4.1. Study population

The study population was consisting of seven patients with aortic or pulmonar stenosis and two controls. All patients were imaged with clinical indications and had a stenotic heart valve incorporating flow speed of at least 250 cm/s. The study is a part of larger Helsinki Medical Imaging Center´s project on improving the quality of cardiac magnetic resonance studies. The study had a permission of the institutional ethics committee.

4.2. Phase contrast flow imaging

Imaging was done with a 1.5T Siemens Avanto scanner (Siemens Medical, Erlangen, Germany). Standard 6 channel body coil with 6 channel spine coil was used with all patients. Cardiac gating was done with a standard remote sensor package using three electrode VCG system.

Phase contrast flow imaging protocol was as follows: First, the in plane phase contrast measurement was carried out along the left and right outflow tract to assess the velocity and the direction of the flow. Alignment of the in-plane measurement was done with the help of anatomical 2-chamber, 4-chamber, short axis and left or right ventricular outflow tract cine images. The magnitude image of the in-plane measurement was used to verify the location of the valve and in-plane phase contrast image was used to estimate the peak flow velocity. Also, the direction of the jet was verified in the case of considerable variation from the outflow tract direction to avoid error caused by measurement plane misalignment. Through-plane measurements were then done with 3-5 different distances from the valve (Figure 30). All the planes were parallel and placed successively 6 mm apart from each other. The number of the planes were limited by the length of the tract allowing free progress of the jet.

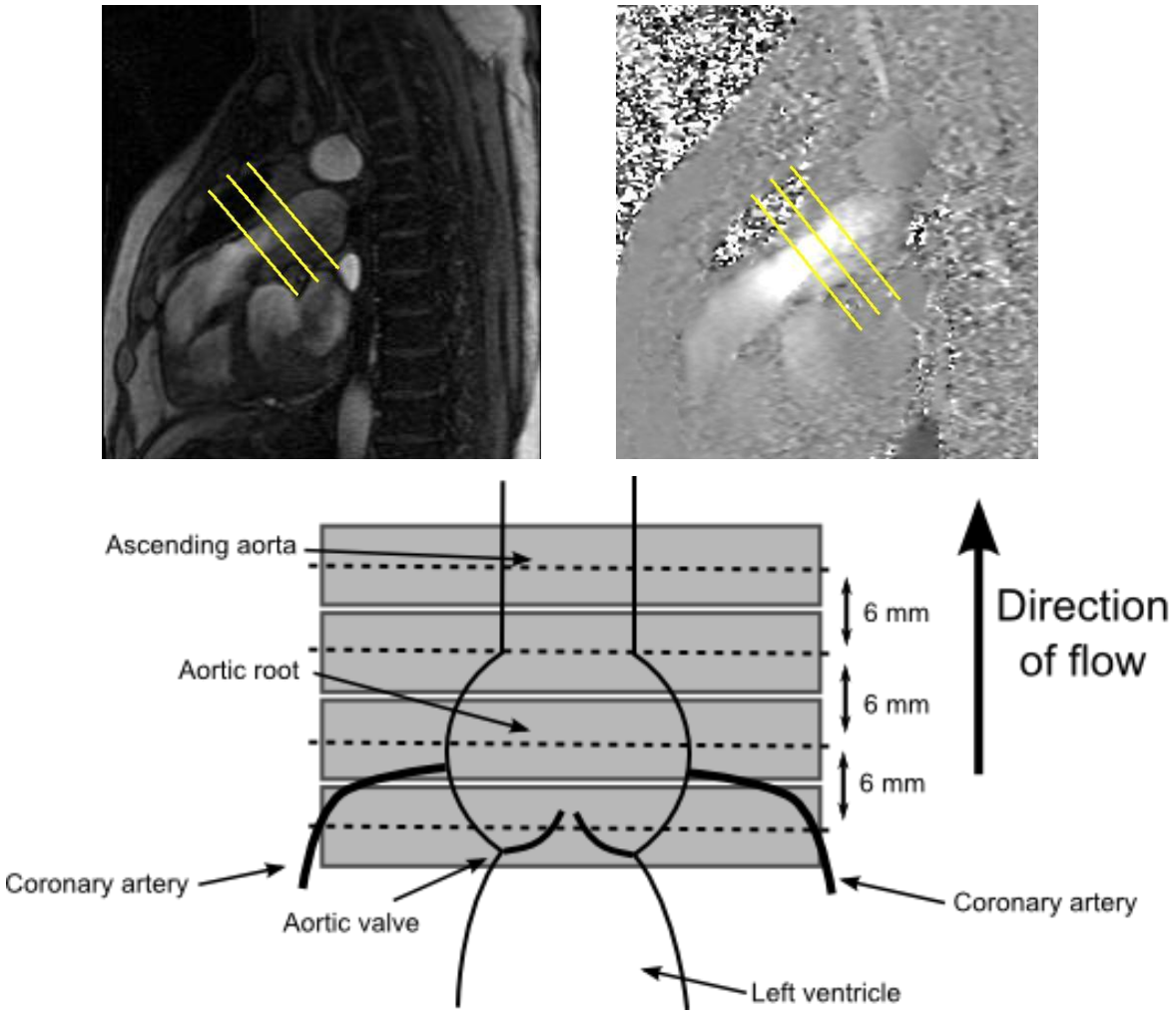

Figure 30. Illustration of the used slice positioning. Magnitude image on the top left, phase image on the top right and the schematic diagram of the slice positioning in case of 4 image slices on the bottom.

Flow images were acquired in a single breath hold with a phase contrast fast gradient echo pulse sequence using GRAPPA parallel imaging factor of two. The acquisition parameters are presented in Table 1. The V_{ENC} values varied between 275-450 cm/s with patients and 100-150 cm/s with controls. The duration of the breath hold was approximately 20s depending on the heart rate of the patient.

Table 1. Sequence parameters.

	in-plane	through-plane
TR (ms)	9,6	12,2
TE (ms)	2,1	3,1
Slice thickness (mm)	5,5	6
Acquisition matrix	192 x 192	256 x 256
FOV (mm)	320 x 320	320 x 320
Flip angle (degrees)	30	30
Image frames	20	20

4.3. Phase contrast image analysis

The phase contrast image data was analyzed with the Argus software (Siemens Medical Systems, Erlangen, Germany). The ROI was determined in the cardiac phase containing the largest flow volume and extended to other image frames with the contour sensing feature of the program. Contours were corrected manually before the actual measurement in case of artifacts near the area of interest [112]. The stroke volume was calculated with the ARGUS analyzation software (Siemens Medical, Erlangen, Germany) by determining the amount of flow in each phase and summing up the flow volumes. The position of the imaging plane relative to the valve was observed at the end of the systolic phase to detect the most distal position of the valve.

The interobserver reproducibility of the flow volume measurements was evaluated in 6 patients and 2 volunteers. Two independent observers measured the amount of flow in all scanned planes. A correlation coefficient was then calculated for the measurements [113].

4.4. Static phantom

A static gelatine phantom was used to assess hardware induced flow offset in the used scanner. The phantom was built by filling 10 liter plastic container with 5mmol/l of Gd-DTPA doped gelatine. The phantom was placed at the position where it lies approximately in the place of patients heart during CMR study. After that, three phase contrast flow images were taken in transversal direction distributed equally along the phantom. The used image parameters were the same presented in Table 1 for the through-plane images. Venc value of 400 cm/s was used in imaging to imitate the

conditions when imaging a patient with stenotic heart valve. In each slice the amount of mean flow velocity offset were measured in 5 locations as presented in Figure 31. The size of each circular region of interest (ROI) was approximately 8 cm^2 imitating typical cross-sectional area of the left or right outflow tract.

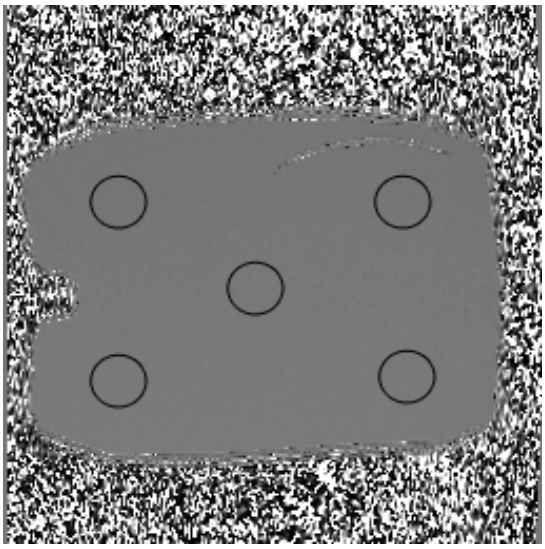

Figure 31. Phase contrast image of the static gel phantom. Used ROIs marked with black circles.

5. Results

Measured relative stroke volumes against the measurement plane distance from the valve are presented in Figure 32. In stenotic cases measured stroke volumes were found to vary 10-25% within a centimeter contrary to the volunteers where measured stroke volume varied less than 10% in the same range. In patient group, the peak stroke volume was measured 1.3-2.5 cm distal to the valve in 5 out of 7 patients. In two case the measurement plane location with peak flow volume could not be measured due to morphological restrictions. In one control the flow volume measured closest to the valve wall is likely effected by valve movement. Stroke volumes and flow velocities of the patients are presented in Table 2.

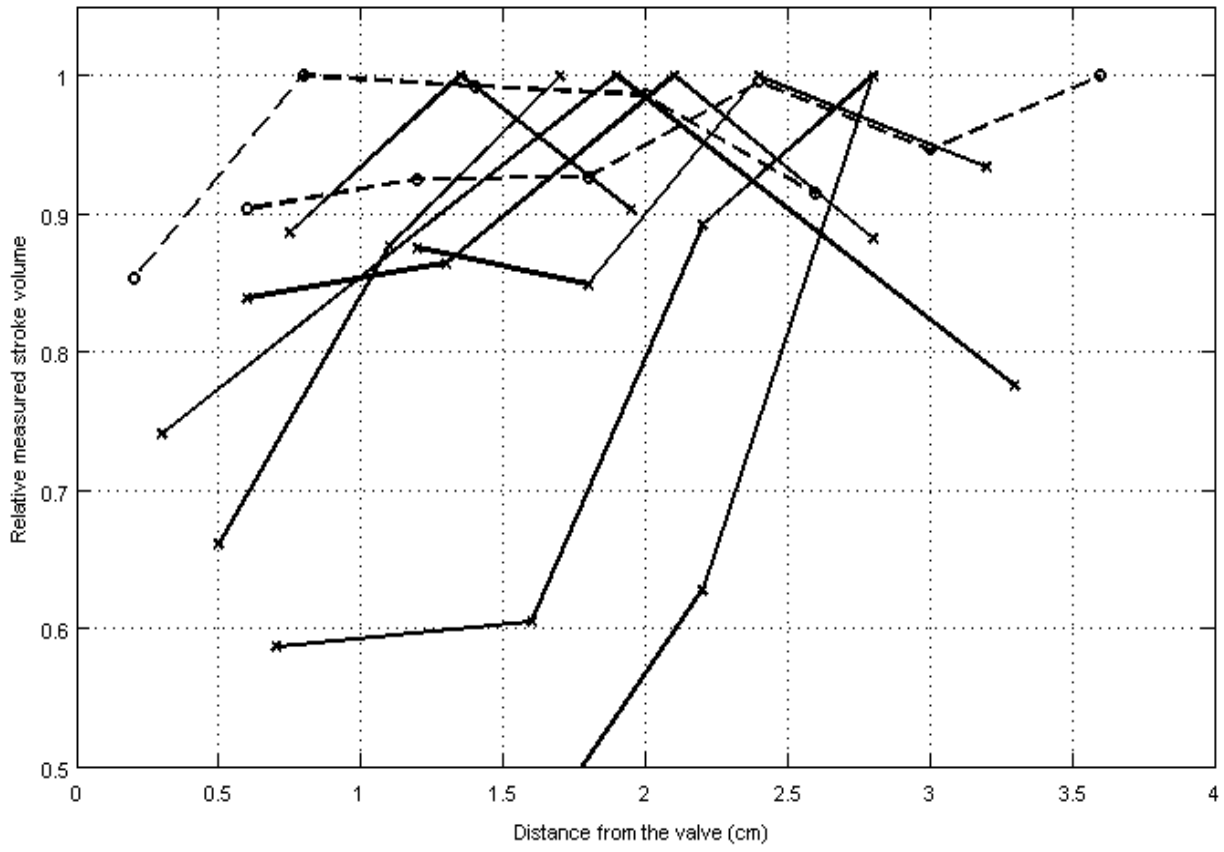

Figure 32. Measured stroke volumes plotted against the measurement plane distance from the valve. Volumes measured in case of stenotic arteries marked with continuous line and controls with normal morphology marked with broken line.

Table 2. Stroke volume and peak flow velocity statistics of the patient group.

	mean	SD	range
Stroke volume	108.0 ml	24.4 ml	72.1 - 133.4 ml
Flow velocity	346.5 cm/s	75.8 cm/s	265.8 – 433.4 cm/s

The correlation coefficient in the intraobserver flow volume measurements was found to be 0.95 ($p<0.0001$) .

The mean flow velocity offset measured with all the ROIs in the phantom was 0.7 cm/s with standard deviation of 3.3 cm/s and a range of -3.7 - 9 cm/s. The offset was considerably smaller in the subgroup of ROIs consisting only ones in the middle of each image slice where the mean offset was 0.3 cm/s and the standard deviation 1.1 cm/s.

6. Discussion

Measurement of the stroke volume in the presence of stenotic flow is prone to numerous errors. The key to successful flow study is to recognize error factors and minimize their effect by adjusting imaging parameters and taking physiological elements into account. In this study the effect of the image plane distance to the valve on measured stroke volume has been investigated. The image plane distance from the valve has a major impact on the amount of acceleration artifact and partial volume effects. It was found that there is an optimal measurement region and it is not substantially altering between the patients. In stenotic patients with accelerated aortic or pulmonal flow the optimal slice is approximately 2 cm distal to the valve. Without further knowledge of the present flow patterns, this should be a valid guideline to decrease measurement error. However, in case of complex morphology or extreme flow speed, it has to be accepted that the optimal measurement plane may be impossible to achieve and approximately 10-25% error originating from non-optimal slice positioning can be present. The estimated amount of stroke volume measurement error caused by different sources is presented in Table 3.

Table 3. Effect of the error sources involved in phase contrast stroke volume measurement approximated with flow speed 400 cm/s and the used sequence properties.

Source of error	Amount of error
Slice position	10-25% [1]
Slice alignment	4% [2]
Eddy currents	10% [3]
	4% [4]
Valve movement	7% [5]
Temporal resolution	5% [6]

[1] As presented in this study
[2] 20 degree misalignment. Greil et al. [102]
[3] Gatehouse et al. [105] and Rolf et al. [106]
[4] Phantom measurements
[5] According to systolic volume measurements by Kozerke et al. [72, 73]
[6] With 16 image frames per heart cycle. Garcia et al. [104]

The underestimation of the flow measured immediately after the heart valve is most likely caused by acceleration artifact. The used bipolar gradients are producing error if the speed of the flow is changing in the vicinity of image slice. The theoretical effective range of acceleration artifact can be determined if the duration of the flow encoding bipolar gradient is known. Assuming that the flow encoding gradient is switched on immediately after the slice selective RF pulse, the effective range is close to the product of TE and peak flow velocity. In the case of high flow speed of 400 cm/s, this range extends to 1.2 cm with TE time of 3.1 ms used in the through-plane measurements. In this study, we found that the maximum measured stroke volume is achieved in a plane even further from the valve. This may also result partly from flow pattern changes due to the moving heart valve. When the measurement plane distance from the valve is increased, partial volume effects inflicted by turbulent flow are becoming a dominating factor effecting measured stroke volume [97]. This is most likely producing the evident decrease in measured stroke volumes with measurement plane to valve ranges extending over 2 cm.

There was no access to sophisticated valve position mapping sequences which could increase the accuracy of the results. In a recent study by Kozerke et al. the typical valve movement during one R-R interval was measured to be 12 mm [73]. In this study slices were positioned with the help of in-plane cine images representing the systolic phase to avoid the direct effects of valve movement.

The phantom phase offset correction method presented by Holland et al. [110] was tested, but it was not utilized in this study. The offset correction capability of the method is unarguable, but the method itself may become too time consuming for clinical use. The amount of eddy current offset was noted to be relatively small in our imaging system which decreases the benefits of the use of phantom phase correction in routine use. In the presented phantom measurements the mean velocity offset was 0.7cm/s. With of 80 heartbeats/min and typical 8 cm^2 circular ROI this would produce an error of 4.2 ml in the stroke volume representing approximately 4% error with the mean stroke volume obtained in this study. However, despite the same sequence parameters were used in the phantom study as in the patient study, there is still an important difference in the setups. Scanner fine tunes magnetic field before scanning to match the each subject of study individually. Thus, the exact amount of eddy currents

and phase offset is also different for every patient. The used phantom is small and evenly composed compared with human thoracic area and thus constant field in the phantom is easier to achieve. It is likely that the used scanner produces larger flow velocity offsets in a patient study compared to the phantom study. Nevertheless, obtained phantom results represent a rough estimate for hardware produced error in the used scanner.

Despite complex flow patterns, the interobserver variability of data analysis was found to be low. Also, there was almost no difference in the interobserver correlation between the patients and volunteers regardless of the major differences in the flow and morphology characteristics.

The size of study population may limit results applicability to patients. Larger patient and control population are needed to be able to use a statistical approach to determine an optimal measurement plane.

7. Conclusions

Phase contrast velocity encoded imaging provides a powerful non-invasive and non-ionizing method for quantifying blood flow inside the human body. Nowadays even smaller vessels can be studied and less patient cooperation is needed. However, due to the technical complexity of MRI, it is important to understand the error mechanisms affecting the accuracy of the results. Some of the error mechanisms are originating from the physiological and anatomical conditions not always optimal for imaging. Other sources of error are present because of the physical limitations in hardware. Some processes may be simply too fast or small to be captured with the phase contrast method. There are many methods for reducing the errors. Most of these methods are embedded in the imaging process and are relatively invisible to the user. Some, on the other hand, are relying on special equipment and operator´s skill to take each patient into account individually.

In the presented study the effect of the image plane position on measured stroke volume was measured. It was found that in case of accelerated flow there is less error if the image plane is placed approximately 2 cm distal to the cardiac valve. If the image plane was placed close to the cardiac valve or further down the flow tract, the error was considerably larger. Such connection between the slice location and measured stroke volume was not found in controls. The results can be applied to clinical work to decrease flow measurement error by 10-25% in cases with accelerated flow.

8. References

[1] P. R. Moran, “A flow velocity zeugmatographic interlace for NMR imaging in humans,” *Magnetic Resonance Imaging*, vol. 1, pp. 197–203, Jan. 1982.

[2] S. D. Caruthers, S. J. Lin, P. Brown, M. P. Watkins, T. A. Williams, K. A. Lehr, and S. A. Wickline, “Practical Value of Cardiac Magnetic Resonance Imaging for Clinical Quantification of Aortic Valve Stenosis,” *Circulation*, vol. 108, pp. 2236–2243, Nov. 2003.

[3] G. P. Chatzimavroudis, J. N. Oshinski, R. H. Franch, P. G. Walker, A. P. Yoganathan, and R. I. Pettigrew, “Evaluation of the Precision of Magnetic Resonance Phase Velocity Mapping for Blood Flow Measurements,” *J Cardiovasc Magn Reson*, vol. 3, pp. 11–19, Jan. 2001.

[4] V. S. Lee, C. E. Spritzer, B. A. Carroll, L. G. Pool, M. A. Bernstein, S. K. Heinle, and J. R. MacFall, “Flow quantification using fast cine phase-contrast MR imaging, conventional cine phase-contrast MR imaging, and Doppler sonography: in vitro and in vivo validation.,” *American Journal of Roentgenology*, vol. 169, pp. 1125–1131, Oct. 1997.

[5] S. R. Underwood, D. N. Firmin, R. H. Klipstein, R. S. Rees, and D. B. Longmore, “Magnetic resonance velocity mapping: clinical application of a new technique.,” *British Heart Journal*, vol. 57, pp. 404–412, May 1987.

[6] P. Gatehouse, J. Keegan, L. Crowe, S. Masood, R. Mohiaddin, K.-F. Kreitner, and D. Firmin, “Applications of phase-contrast flow and velocity imaging in cardiovascular MRI,” *European radiology*, vol. 15, pp. 2172–2184, Oct. 2005.

[7] J. Lotz, C. Meier, A. Leppert, and M. Galanski, “Cardiovascular Flow Measurement with Phase-Contrast MR Imaging: Basic Facts and Implementation1,” *Radiographics*, vol. 22, pp. 651–671, May 2002.

[8] F. Grothues, J. C. Moon, N. G. Bellenger, G. S. Smith, H. U. Klein, and D. J. Pennell, “Interstudy reproducibility of right ventricular volumes, function, and mass with cardiovascular magnetic resonance,” *American Heart Journal*, vol. 147, pp. 218–223, Feb. 2004.

[9] P. J. Kilner, P. D. Gatehouse, and D. N. Firmin, “Flow Measurement by Magnetic Resonance: A Unique Asset Worth Optimising,” *J Cardiovasc Magn Reson*, vol. 9, pp. 723–728, Jan. 2007.

[10] Y. Richter and E. R. Edelman, “Cardiology Is Flow,” *Circulation*, vol. 113, pp. 2679–2682, June 2006.

[11] K. Wong, R. Kelso, S. Worthley, P. Sanders, J. Mazumdar, and D. Abbott, “Cardiac Flow Analysis Applied to Phase Contrast Magnetic Resonance Imaging of the Heart,” *Annals of Biomedical Engineering*, vol. 37, no. 8, pp. 1495–1515, 2009.

[12] C. Elkins and M. Alley, “Magnetic resonance velocimetry: applications of magnetic resonance imaging in the measurement of fluid motion,” vol. 43, no. 6, pp. 823–858, 2007.

[13] B. Jung, B. Schneider, M. Markl, B. Saurbier, A. Geibel, and J. Hennig, “Measurement of Left Ventricular Velocities: Phase Contrast MRI Velocity Mapping Versus Tissue-Doppler-Ultrasound in Healthy Volunteers,” *J Cardiovasc Magn Reson*, vol. 6, pp. 777–783, Jan. 2004.

[14] P. J. Kilner, T. Geva, H. Kaemmerer, P. T. Trindade, J. Schwitter, and G. D. Webb, “Recommendations for cardiovascular magnetic resonance in adults with congenital heart disease from the respective working groups of the European Society of Cardiology,” *European Heart Journal*, vol. 31, pp. 794–805, Apr. 2010.

[15] R. H. Klipstein, D. N. Firmin, S. R. Underwood, R. S. Rees, and D. B. Longmore, “Blood flow patterns in the human aorta studied by magnetic resonance.,” *British Heart Journal*, vol. 58, pp. 316–323, Oct. 1987.

[16] P. Masci, S. Dymarkowski, and J. Bogaert, “Valvular heart disease: what does cardiovascular MRI add?,” vol. 18, no. 2, pp. 197–208, 2008.

[17] S. Muzzarelli, A. K. Meadows, K. G. Ordovas, M. D. Hope, C. B. Higgins, J. C. Nielsen, T. Geva, and J. J. Meadows, “Prediction of Hemodynamic Severity of Coarctation by Magnetic Resonance Imaging,” *The American Journal of Cardiology*, vol. 108, pp. 1335–1340, Nov. 2011.

[18] D. H. Szolar, H. Sakuma, and C. B. Higgins, “Cardiovascular applications of magnetic resonance flow and velocity measurements,” *J. Magn. Reson. Imaging*, vol. 6, pp. 78–89, Jan. 1996.

[19] P. J. Kilner, C. C. Manzara, R. H. Mohiaddin, D. J. Pennell, M. G. Sutton, D. N. Firmin, S. R. Underwood, and D. B. Longmore, “Magnetic resonance jet velocity mapping in mitral and aortic valve stenosis.,” *Circulation*, vol. 87, pp. 1239–1248, Apr. 1993.

[20] P. Dyverfeldt, A. Sigfridsson, J.-P. E. Kvitting, and T. Ebbers, “Quantification of intravoxel velocity standard deviation and turbulence intensity by generalizing phase-contrast MRI,” *Magn. Reson. Med.*, vol. 56, no. 4, pp. 850–858, 2006.

[21] M. Jeltsch, S. Ranft, O. Klass, A. J. Aschoff, and M. H. K. Hoffmann, “Evaluation of Accordance of Magnetic Resonance Volumetric and Flow Measurements in Determining Ventricular Stroke Volume in Cardiac Patients,” *Acta Radiol*, vol. 49, pp. 530–539, Jan. 2008.

[22] P. J. Cawley, J. H. Maki, and C. M. Otto, “Cardiovascular Magnetic Resonance Imaging for Valvular Heart Disease,” *Circulation*, vol. 119, pp. 468–478, Jan. 2009.

[23] W. G. Hundley, H. F. Li, J. E. Willard, C. Landau, R. A. Lange, B. M. Meshack, L. D. Hillis, and R. M. Peshock, “Magnetic Resonance Imaging Assessment of the Severity of Mitral Regurgitation,” *Circulation*, vol. 92, pp. 1151–1158, Sept. 1995.

[24] J. W. Koskenvuo, V. Järvinen, J. P. Pärkkä, T. O. Kiviniemi, and J. J. Hartiala, “Cardiac magnetic resonance imaging in valvular heart disease,” *Clinical Physiology and Functional Imaging*, vol. 29, no. 4, pp. 229–240, 2009.

[25] J.-P. E. Kvitting, T. Ebbers, L. Wigström, J. Engvall, C. L. Olin, and A. F. Bolger, “Flow patterns in the aortic root and the aorta studied with time-resolved, 3-dimensional, phase-contrast magnetic resonance imaging: implications for aortic valveâ€“sparing surgery,” *The Journal of Thoracic and Cardiovascular Surgery*, vol. 127, pp. 1602–1607, June 2004.

[26] G. Sommer, J. Bremerich, and G. Lund, "Magnetic resonance imaging in valvular heart disease: Clinical application and current role for patient management," *J. Magn. Reson. Imaging*, vol. 35, no. 6, pp. 1241–1252, 2012.

[27] M. I. Boechat, O. Ratib, P. L. Williams, A. S. Gomes, J. S. Child, and V. Allada, "Cardiac MR imaging and MR angiography for assessment of complex tetralogy of Fallot and pulmonary atresia.," *Radiographics : a review publication of the Radiological Society of North America, Inc*, vol. 25, no. 6, pp. 1535–1546, 2005.

[28] U. K. Chowdhury, K. K. Pradeep, C. D. Patel, R. Singh, A. S. Kumar, B. Airan, G. S. Gulati, S. S. Kothari, A. Saxena, M. Kalaivani, and P. Venugopal, "Noninvasive Assessment of Repaired Tetralogy of Fallot by Magnetic Resonance Imaging and Dynamic Radionuclide Studies," *The Annals of Thoracic Surgery*, vol. 81, pp. 1436–1442, Apr. 2006.

[29] T. Geva, B. M. Sandweiss, K. Gauvreau, J. E. Lock, and A. J. Powell, "Factors associated with impaired clinical status in long-term survivors of tetralogy of Fallot repair evaluated by magnetic resonance imaging," *Journal of the American College of Cardiology*, vol. 43, pp. 1068–1074, Mar. 2004.

[30] T. Oosterhof, B. J. M. Mulder, H. W. Vliegen, and A. de Roos, "Cardiovascular magnetic resonance in the follow-up of patients with corrected tetralogy of Fallot: A review," *American Heart Journal*, vol. 151, pp. 265–272, Feb. 2006.

[31] A. J. Powell and T. Geva, "Blood Flow Measurement by Magnetic Resonance Imaging in Congenital Heart Disease," vol. 21, no. 1, pp. 47–58, 2000.

[32] A. E. van der Hulst, J. J. M. Westenberg, L. J. M. Kroft, J. J. Bax, N. A. Blom, A. de Roos, and A. A. W. Roest, "Tetralogy of Fallot: 3D Velocity-encoded MR Imaging for Evaluation of Right Ventricular Valve Flow and Diastolic Function in Patients after Correction1," *Radiology*, vol. 256, pp. 724–734, Sept. 2010.

[33] "Conditions We Treat: Tetralogy of Fallot - http://med.umich.edu/Mott/congenital/services/patient_con_tet.html."

[34] A. Hsiao, M. Alley, P. Massaband, R. Herfkens, F. Chan, and S. Vasanawala, "Improved cardiovascular flow quantification with time-resolved volumetric phase-contrast MRI," *Pediatric Radiology*, vol. 41, pp. 711–720, Jan. 2011.

[35] M. Markl, F. P. Chan, M. T. Alley, K. L. Wedding, M. T. Draney, C. J. Elkins, D. W. Parker, R. Wicker, C. A. Taylor, R. J. Herfkens, and N. J. Pelc, "Time-resolved three-dimensional phase-contrast MRI," *J. Magn. Reson. Imaging*, vol. 17, no. 4, pp. 499–506, 2003.

[36] M. Markl, M. T. Draney, D. C. Miller, J. M. Levin, E. E. Williamson, N. J. Pelc, D. H. Liang, and R. J. Herfkens, "Time-resolved three-dimensional magnetic resonance velocity mapping of aortic flow in healthy volunteers and patients after valve-sparing aortic root replacement," *The Journal of Thoracic and Cardiovascular Surgery*, vol. 130, pp. 456–463, Aug. 2005.

[37] M. Markl, W. Wallis, and A. Harloff, "Reproducibility of flow and wall shear stress analysis using flow-sensitive four-dimensional MRI," *J. Magn. Reson. Imaging*, vol. 33, pp. 988–994, Apr. 2011.

[38] L. Wigström, T. Ebbers, A. Fyrenius, M. Karlsson, J. Engvall, B. Wranne, and A. F. Bolger, "Particle trace visualization of intracardiac flow using time-resolved 3D phase contrast MRI," *Magn. Reson. Med.*, vol. 41, no. 4, pp. 793–799, 1999.

[39] L. Wigström, L. Sjöqvist, and B. Wranne, "Temporally resolved 3D phase-contrast imaging," *Magn. Reson. Med.*, vol. 36, no. 5, pp. 800–803, 1996.

[40] B. F. Geerts, L. P. Aarts, and J. R. Jansen, "Methods in pharmacology: measurement of cardiac output," *British Journal of Clinical Pharmacology*, vol. 71, no. 3, pp. 316–330, 2011.

[41] L. A. H. Critchley and J. A. J. H. Critchley, "A Meta-Analysis of Studies Using Bias and Precision Statistics to Compare Cardiac Output Measurement Techniques," *Journal of Clinical Monitoring and Computing*, vol. 15, pp. 85–91, Feb. 1999.

[42] A. Iskandrian, “Validation of left ventricular volume measurements by gated SPECT 99mTc-labeled sestamibi imaging*1,” *Journal of Nuclear Cardiology*, vol. 5, pp. 574–578, Dec. 1998.

[43] K. Rajappan, L. Livieratos, P. G. Camici, and D. J. Pennell, “Measurement of Ventricular Volumes and Function: A Comparison of Gated PET and Cardiovascular Magnetic Resonance,” *Journal of Nuclear Medicine*, vol. 43, pp. 806–810, June 2002.

[44] *Principles of magnetic resonance imaging : a signal processing perspective*, SPIE Optical Engineering Press ; IEEE Press, 2000.

[45] S. Balter, “An introduction to the physics of magnetic resonance imaging.,” *Radiographics : a review publication of the Radiological Society of North America, Inc*, vol. 7, pp. 371–383, Mar. 1987.

[46] D. B. Plewes and W. Kucharczyk, “Physics of MRI: A primer,” *J. Magn. Reson. Imaging*, vol. 35, no. 5, pp. 1038–1054, 2012.

[47] J. Ridgway, “Cardiovascular magnetic resonance physics for clinicians: part I,” *Journal of Cardiovascular Magnetic Resonance*, vol. 12, no. 1, pp. 71+, 2010.

[48] M. A. Bernstein, J. Huston, and H. A. Ward, “Imaging artifacts at 3.0T,” *J. Magn. Reson. Imaging*, vol. 24, pp. 735–746, Oct. 2006.

[49] O. Dietrich, M. F. Reiser, and S. O. Schoenberg, “Artifacts in 3-T MRI: Physical background and reduction strategies,” *European Journal of Radiology*, vol. 65, pp. 29–35, Jan. 2008.

[50] E. Pusey, R. B. Lufkin, R. K. Brown, M. A. Solomon, D. D. Stark, R. W. Tarr, and W. N. Hanafee, “Magnetic resonance imaging artifacts: mechanism and clinical significance.,” *Radiographics*, vol. 6, pp. 891–911, Sept. 1986.

[51] J. Zhuo and R. P. Gullapalli, “AAPM/RSNA physics tutorial for residents: MR artifacts, safety, and quality control.,” *Radiographics : a review publication of the Radiological Society of North America, Inc*, vol. 26, pp. 275–297, Jan. 2006.

[52] D. W. McRobbie, *MRI from picture to proton*. Cambridge University Press, 2007.

[53] A. M. Gharib, A. Elagha, and R. I. Pettigrew, “Cardiac Magnetic Resonance at High Field: Promises and Problems,” *Current Problems in Diagnostic Radiology*, vol. 37, pp. 49–56, Mar. 2008.

[54] B. A. Chronik and B. K. Rutt, “A comparison between human magnetostimulation thresholds in whole-body and head/neck gradient coils,” *Magn. Reson. Med.*, vol. 46, pp. 386–394, Aug. 2001.

[55] B. A. Chronik and B. K. Rutt, “Simple linear formulation for magnetostimulation specific to MRI gradient coils,” *Magn. Reson. Med.*, vol. 45, pp. 916–919, May 2001.

[56] K. P. Pruessmann, M. Weiger, and P. Boesiger, “Sensitivity Encoded Cardiac MRI,” *J Cardiovasc Magn Reson*, vol. 3, pp. 1–9, Jan. 2001.

[57] J. Biglands, A. Radjenovic, and J. Ridgway, “Cardiovascular magnetic resonance physics for clinicians: part II,” *Journal of Cardiovascular Magnetic Resonance*, vol. 14, no. 1, pp. 66+, 2012.

[58] K. R. O’Brien, *Understanding and measuring flow in aortic stenosis with MRI*. PhD thesis, 2009.

[59] D. N. Ku, “Blood flow in arteries,” *Annual Review of Fluid Mechanics*, vol. 29, no. 1, pp. 399–434, 1997.

[60] S. A. Berger and L. D. Jou, “Flows in Stenotic Vessels,” *Annual Review of Fluid Mechanics*, vol. 32, no. 1, pp. 347–382, 2000.

[61] P. Dyverfeldt, J.-P. E. Kvitting, A. Sigfridsson, J. Engvall, A. F. Bolger, and T. Ebbers, “Assessment of fluctuating velocities in disturbed cardiovascular blood flow: In vivo feasibility of generalized phase-contrast MRI,” *J. Magn. Reson. Imaging*, vol. 28, no. 3, pp. 655–663, 2008.

[62] P. D. Stein and H. N. Sabbah, “Turbulent blood flow in the ascending aorta of humans with normal and diseased aortic valves.,” *Circulation Research*, vol. 39, pp. 58–65, July 1976.

[63] T. Frauenrath, K. Fuchs, M. A. Dieringer, C. Özerdem, N. Patel, W. Renz, A. Greiser, T. Elgeti, and T. Niendorf, "Detailing the use of magnetohydrodynamic effects for synchronization of MRI with the cardiac cycle: A feasibility study," *J. Magn. Reson. Imaging*, vol. 36, no. 2, pp. 364–372, 2012.

[64] J. W. Krug and G. Rose, "Magnetohydrodynamic distortions of the ECG in different MR scanner configurations," in *Computing in Cardiology, 2011*, pp. 769–772, IEEE, 2011.

[65] M. S. Nacif, A. Zavodni, N. Kawel, E.-Y. Choi, J. a. A. C. Lima, and D. A. Bluemke, "Cardiac magnetic resonance imaging and its electrocardiographs (ECG): tips and tricks," *The International Journal of Cardiovascular Imaging (formerly Cardiac Imaging)*, vol. 28, pp. 1465–1475, Aug. 2012.

[66] T. Frauenrath, F. Hezel, U. Heinrichs, S. Kozerke, J. F. Utting, M. Kob, C. Butenweg, P. Boesiger, and T. Niendorf, "Feasibility of cardiac gating free of interference with electro-magnetic fields at 1.5 Tesla, 3.0 Tesla and 7.0 Tesla using an MR-stethoscope.," *Investigative radiology*, vol. 44, pp. 539–547, Sept. 2009.

[67] A. C. Larson, R. D. White, G. Laub, E. R. McVeigh, D. Li, and O. P. Simonetti, "Self-gated cardiac cine MRI," *Magn. Reson. Med.*, vol. 51, pp. 93–102, Jan. 2004.

[68] S. Ley, J. Ley-Zaporozhan, K.-F. Kreitner, S. Iliyushenko, M. Puderbach, W. Hosch, H. Wenz, J.-P. Schenk, and H.-U. Kauczor, "MR flow measurements for assessment of the pulmonary, systemic and bronchosystemic circulation: Impact of different ECG gating methods and breathing schema," *European Journal of Radiology*, vol. 61, pp. 124–129, Jan. 2007.

[69] E. Frank, "An Accurate, Clinically Practical System For Spatial Vectorcardiography," *Circulation*, vol. 13, pp. 737–749, May 1956.

[70] J. W. Krug, G. Rose, D. Stucht, G. Clifford, and J. Oster, "Limitations of VCG based gating methods in ultra high field cardiac MRI," *Journal of Cardiovascular Magnetic Resonance*, vol. 15, no. Suppl 1, pp. W19+, 2013.

[71] J. Malmivuo and R. Plonsey, *Bioelectromagnetism : principles and applications of bioelectric and biomagnetic fields*. Oxford University Press, 1995.

[72] S. Kozerke, J. Schwitter, E. M. Pedersen, and P. Boesiger, "Aortic and mitral regurgitation: Quantification using moving slice velocity mapping," *J. Magn. Reson. Imaging*, vol. 14, no. 2, pp. 106–112, 2001.

[73] S. Kozerke, M. B. Scheidegger, E. M. Pedersen, and P. Boesiger, "Heart motion adapted cine phase-contrast flow measurements through the aortic valve," *Magn. Reson. Med.*, vol. 42, no. 5, pp. 970–978, 1999.

[74] M. Beer, H. Stamm, W. Machann, A. Weng, J. P. Goltz, F. Breunig, F. Weidemann, D. Hahn, and H. Köstler, "Free breathing cardiac real-time cine MR without ECG triggering," *International Journal of Cardiology*, vol. 145, pp. 380–382, Nov. 2010.

[75] M. A. Bolen, R. M. Setser, R. S. Gabriel, R. D. Renapurkar, Y. Tandon, M. L. Lieber, M. Y. Desai, and S. D. Flamm, "Effect of protocol choice on phase contrast cardiac magnetic resonance flow measurement in the ascending aorta: breath-hold and non-breath-hold," *The International Journal of Cardiovascular Imaging (formerly Cardiac Imaging)*, pp. 1–8, Apr. 2012.

[76] S. Ley, C. Fink, M. Puderbach, J. Zaporozhan, C. Plathow, M. Eichinger, W. Hosch, K.-F. Kreitner, and H.-U. Kauczor, "MRI Measurement of the Hemodynamics of the Pulmonary and Systemic Arterial Circulation: Influence of Breathing Maneuvers," *American Journal of Roentgenology*, vol. 187, pp. 439–444, Aug. 2006.

[77] H. Sakuma, N. Kawada, H. Kubo, Y. Nishide, K. Takano, N. Kato, and K. Takeda, "Effect of breath holding on blood flow measurement using fast velocity encoded cine MRI," *Magn. Reson. Med.*, vol. 45, no. 2, pp. 346–348, 2001.

[78] H. Kandpal, R. Sharma, K. S. Madhusudhan, and K. S. Kapoor, "Respiratory-Triggered Versus Breath-Hold Diffusion-Weighted MRI of Liver Lesions: Comparison of Image Quality and Apparent Diffusion Coefficient Values," *American Journal of Roentgenology*, vol. 192, pp. 915–922, Apr. 2009.

[79] M. L. Chuang, M. H. Chen, V. C. Khasgiwala, M. V. McConnell, R. R. Edelman, and W. J. Manning, "Adaptive correction of imaging plane position in segmented K-space cine cardiac MRI," *J. Magn. Reson. Imaging*, vol. 7, no. 5, pp. 811–814, 1997.

[80] D. Firmin and J. Keegan, "Navigator Echoes in Cardiac Magnetic Resonance," *J Cardiovasc Magn Reson*, vol. 3, pp. 183–193, Jan. 2001.

[81] C. Baltes, S. Kozerke, D. Atkinson, and P. Boesiger, "Retrospective Respiratory Motion Correction for Navigated Cine Velocity Mapping," *J Cardiovasc Magn Reson*, vol. 6, pp. 785–792, Jan. 2004.

[82] K. Isaaz, J. F. Bruntz, A. Da Costa, D. Winninger, A. Cerisier, C. de Chillou, N. Sadoul, M. Lamaud, G. Ethevenot, and E. Aliot, "Noninvasive quantitation of blood flow turbulence in patients with aortic valve disease using online digital computer analysis of Doppler velocity data," *Journal of the American Society of Echocardiography*, vol. 16, pp. 965–974, Sept. 2003.

[83] N. M. Rajamannan, "Calcific Aortic Stenosis," *Arteriosclerosis, Thrombosis, and Vascular Biology*, vol. 29, pp. 162–168, Feb. 2009.

[84] F. Robicsek, M. J. Thubrikar, J. W. Cook, and B. Fowler, "The congenitally bicuspid aortic valve: how does it function? Why does it fail?," *The Annals of Thoracic Surgery*, vol. 77, pp. 177–185, Jan. 2004.

[85] M. W. Kon, S. G. Myerson, N. E. Moat, and D. J. Pennell, "Quantification of regurgitant fraction in mitral regurgitation by cardiovascular magnetic resonance: comparison of techniques.," *The Journal of heart valve disease*, vol. 13, pp. 600–607, July 2004.

[86] A. P. Yoganathan, K. B. Chandran, and F. Sotiropoulos, "Flow in Prosthetic Heart Valves: State-of-the-Art and Future Directions," *Annals of Biomedical Engineering*, vol. 33, pp. 1689–1694, Dec. 2005.

[87] P. Pibarot and J. G. Dumesnil, "Prosthetic Heart Valves: Selection of the Optimal Prosthesis and Long-Term Management," *Circulation*, vol. 119, pp. 1034–1048, Feb. 2009.

[88] M.-B. Edwards, K. M. Taylor, and F. G. Shellock, “Prosthetic heart valves: Evaluation of magnetic field interactions, heating, and artifacts at 1.5 T,” *J. Magn. Reson. Imaging*, vol. 12, pp. 363–369, Aug. 2000.

[89] M. J. van der Laan, L. W. Bartels, C. J. Bakker, M. A. Viergever, and J. D. Blankensteijn, “Suitability of 7 aortic stent-graft models for MRI-based surveillance.,” *Journal of endovascular therapy : an official journal of the International Society of Endovascular Specialists*, vol. 11, pp. 366–371, Aug. 2004.

[90] S. Ringgaard, S. A. Oyre, and E. M. Pedersen, “Arterial MR Imaging Phase-Contrast Flow Measurement: Improvements with Varying Velocity Sensitivity during Cardiac Cycle1,” *Radiology*, vol. 232, pp. 289–294, July 2004.

[91] G. Z. Yang, P. Burger, P. J. Kilner, S. P. Karwatowski, and D. N. Firmin, “Dynamic range extension of cine velocity measurements using motion registered spatiotemporal phase unwrapping,” *J. Magn. Reson. Imaging*, vol. 6, no. 3, pp. 495–502, 1996.

[92] M. B. M. Hofman, F. C. Visser, A. C. Van Rossum, G. Q. M. Vink, M. Sprenger, and N. Westerhof, “In Vivo Validation of Magnetic Resonance Blood Volume Flow Measurements with Limited Spatial Resolution in Small Vessels,” *Magn. Reson. Med.*, vol. 33, pp. 778–784, June 1995.

[93] L. Søndergaard, F. Stahlberg, and C. Thomsen, “Magnetic Resonance Imaging of Valvular Heart Disease,” *J. Magn. Reson. Imaging*, vol. 10, no. 5, pp. 627–638, 1999.

[94] C. Tang, D. D. Blatter, and D. L. Parker, “Accuracy of phase-contrast flow measurements in the presence of partial-volume effects,” *J. Magn. Reson. Imaging*, vol. 3, pp. 377–385, Mar. 1993.

[95] D. Saloner, “The AAPM/RSNA physics tutorial for residents. An introduction to MR angiography.,” *Radiographics*, vol. 15, pp. 453–465, Mar. 1995.

[96] K. R. O’Brien, S. G. Myerson, B. R. Cowan, A. A. Young, and M. D. Robson, “Phase contrast ultrashort TE: A more reliable technique for measurement of high-velocity turbulent stenotic jets,” *Magn. Reson. Med.*, vol. 62, no. 3, pp. 626–636, 2009.

[97] S. Petersson, P. Dyverfeldt, R. Gardhagen, M. Karlsson, and T. Ebbers, "Simulation of phase contrast MRI of turbulent flow," *Magn. Reson. Med.*, vol. 64, no. 4, pp. 1039–1046, 2010.

[98] K. W. Moser, E. C. Kutter, J. G. Georgiadis, R. O. Buckius, H. D. Morris, and J. R. Torczynski, "Velocity measurements of flow through a step stenosis using Magnetic Resonance Imaging," vol. 29, no. 5, pp. 438–447, 2000.

[99] J. N. Oshinski, D. N. Ku, D. E. Bohning, and R. I. Pettigrew, "Effects of acceleration on the accuracy of MR phase velocity measurements," *J. Magn. Reson. Imaging*, vol. 2, pp. 665–670, Nov. 1992.

[100] A. J. Barker, F. Staehle, J. Bock, B. A. Jung, and M. Markl, "Analysis of complex cardiovascular flow with three-component acceleration-encoded MRI," *Magn. Reson. Med.*, vol. 67, pp. 50–61, Jan. 2012.

[101] E. A. Waters, S. D. Caruthers, and S. A. Wickline, "Correlation Analysis of Stenotic Aortic Valve Flow Patterns Using Phase Contrast MRI," *Annals of Biomedical Engineering*, vol. 33, pp. 878–887, July 2005.

[102] G. Greil, T. Geva, S. E. Maier, and A. J. Powell, "Effect of acquisition parameters on the accuracy of velocity encoded cine magnetic resonance imaging blood flow measurements," *J. Magn. Reson. Imaging*, vol. 15, no. 1, pp. 47–54, 2002.

[103] K. R. O'Brien, B. R. Cowan, M. Jain, R. A. H. Stewart, A. J. Kerr, and A. A. Young, "MRI phase contrast velocity and flow errors in turbulent stenotic jets," *J. Magn. Reson. Imaging*, vol. 28, pp. 210–218, July 2008.

[104] J. Garcia, L. Kadem, E. Larose, and P. Pibarot, "In vivo velocity and flow errors quantification by phase-contrast magnetic resonance imaging," in *2008 30th Annual International Conference of the IEEE Engineering in Medicine and Biology Society*, pp. 1377–1380, IEEE, Aug. 2008.

[105] P. D. Gatehouse, M. P. Rolf, M. J. Graves, M. B. M. Hofman, J. Totman, B. Werner, R. A. Quest, Y. Liu, J. von Spiczak, M. Dieringer, D. N. Firmin, A. van Rossum, M. Lombardi, J. Schwitter, J. Schulz-Menger, and P. J. Kilner, "Flow measurement by cardiovascular magnetic resonance: a multi-centre multi-vendor study of background phase offset errors that can compromise the accuracy of derived regurgitant or shunt flow measurements," *Journal of Cardiovascular Magnetic Resonance*, vol. 12, pp. 1–8, Dec. 2010.

[106] M. P. Rolf, M. B. M. Hofman, P. D. Gatehouse, K. Markenroth-Bloch, M. W. Heymans, T. Ebbers, M. J. Graves, J. J. Totman, B. Werner, A. C. van Rossum, P. J. Kilner, and R. M. Heethaar, "Sequence optimization to reduce velocity offsets in cardiovascular magnetic resonance volume flow quantification - A multi-vendor study," *Journal of Cardiovascular Magnetic Resonance*, vol. 13, pp. 1–10, Dec. 2011.

[107] J.-W. Lankhaar, M. B. M. Hofman, J. T. Marcus, J. J. M. Zwanenburg, T. J. C. Faes, and A. Vonk-Noordegraaf, "Correction of phase offset errors in main pulmonary artery flow quantification," *J. Magn. Reson. Imaging*, vol. 22, no. 1, pp. 73–79, 2005.

[108] A. Chernobelsky, O. Shubayev, C. R. Comeau, and S. D. Wolff, "Baseline Correction of Phase Contrast Images Improves Quantification of Blood Flow in the Great Vessels," *J Cardiovasc Magn Reson*, vol. 9, pp. 681–685, Jan. 2007.

[109] D. Giese, M. Haeberlin, C. Barmet, K. P. Pruessmann, T. Schaeffter, and S. Kozerke, "Analysis and correction of background velocity offsets in phase-contrast flow measurements using magnetic field monitoring," *Magn. Reson. Med.*, vol. 67, pp. 1294–1302, May 2012.

[110] B. J. Holland, B. F. Printz, and W. W. Lai, "Baseline correction of phase-contrast images in congenital cardiovascular magnetic resonance.," *Journal of cardiovascular magnetic resonance*, vol. 12, 2010.

[111] M. J. Middione and D. B. Ennis, "Chemical shift-induced phase errors in phase-contrast MRI," *Magn. Reson. Med.*, p. n/a, 2012.

[112] P. Chai and R. Mohiaddin, “How We Perform Cardiovascular Magnetic Resonance Flow Assessment Using Phase-Contrast Velocity Mapping,” *J Cardiovasc Magn Reson*, vol. 7, pp. 705–716, Jan. 2005.

[113] J. L. Rodgers and A. W. Nicewander, “Thirteen Ways to Look at the Correlation Coefficient,” *The American Statistician*, vol. 42, no. 1, pp. 59–66, 1988.